Mitral valve leaflet tissue plasticity following transcatheter edge-to-edge repair in humans

Natalie T. Simonian[a], Carina Gipson[a], Neha Palsikar[a], Nivin Sunesh[a], Sneha Vakamudi[b], Mark J. Pirwitz[b], Robert C. Gorman[c], and Michael S. Sacks[a,1]

[a] *James T. Willerson Center for Cardiovascular Modeling and Simulation*

The Oden Institute for Computational Engineering and Sciences and the Department of Biomedical Engineering

The University of Texas at Austin, Austin, TX, USA

[b] *Ascension Texas Cardiovascular, Austin, TX, USA*

[c] *Gorman-Gillespe Structural Heart*

Keywords: mitral valve, mitral regurgitation, transcatheter edge-to-edge repair, patient-specific, computational modeling, plasticity

---

[1]Corresponding Author: msacks@oden.utexas.edu

ABSTRACT

Transcatheter edge-to-edge repair (TEER) is a promising minimally invasive approach for the treatment of mitral valve (MV) regurgitation (MR). However, long-term outcomes have been suboptimal in several recent clinical trials, likely complicated by the substantial heterogeneity of MR presentations and the combinatorial nature of the procedure itself. Moreover, the long-term consequences of MV TEER on the leaflet tissue itself have never been studied, and represent a key target for procedural optimization. As a first step in addressing these deficiencies, we conducted a novel study to investigate the effects of TEER-induced MV shape and strain at several months after implantation. We first acquired and analyzed longitudinal echocardiographic imaging data from five patients pre, post, and at 3-month follow-up post-TEER. We then quantified TEER-induced time-evolving changes in MV diastolic shape and systolic leaflet strains using a computational in vivo geometry recovery method. In the ED state we found evidence of substantial MV leaflet *plasticity* (defined here as permanent changes MV leaflet geometry) at the 3 month time point. Though the patterns of plasticity were generally heterogeneous, the highest regions of plasticity consistently corresponded to the position of the TEER device. Moreover, the first principal direction field consistently converged onto the position(s) of the clip(s) in all cases, further suggesting that the clip is the primary driver of the observed plasticity. This result emphasized the fact that the MV leaflets are not dimensionally stable post-TEER, and instead continue to remodel. To evaluate the potential confounding effects of concomitant changes in ventricular shape, we also quantified changes in annular and left ventricular dimensions and found no significant changes over time. These observations support our hypothesis that the focal stress concentrations induced by the clip drive MV leaflet tissue remodeling at 3 months. In summary these novel results confirm that TEER has effects beyond those observed immediately post-operation. These unique findings underscore a mechanism for long-term repair failure and constitute a potential key target for patient-specific procedural optimization.

1. INTRODUCTION

Mitral regurgitation (MR) is a valvular disease characterized by improper coaptation of the mitral valve (MV) leaflets, permitting backflow of blood from the left ventricle into the left atrium. MR is the most common valvular disease in the United States, with a prevalence of over 10% in patients over 75 years of age [1, 2]. Without adequate treatment, MR can have debilitating and even lethal consequences, including worsening left ventricular dysfunction, pulmonary congestion, atrial fibrillation, and in certain cases, thromboembolism [3]. In this context, MR is a major prognostic factor of mortality: the risk of mortality with severe MR at five years is 36% and even moderate MR nearly doubles the risk of mortality in patients with multiple cardiac comorbidities [4, 5].

There exists a wide range of treatment options for MR that include pharmacological management, repair, and replacement, with repair preferred when feasible. However, alternatives to invasive repair methods such (e.g. undersized ring annuloplasty) have been sought. Transcatheter edge-to-edge repair (TEER) is a minimally invasive method that first emerged in 2003 as an option for those patients contraindicated for traditional highly invasive surgical interventions [6]. TEER essentially reproduces in the transcatheter format the edge-to-edge repair approach pioneered by Alfieri et al. [7], where the two leaflets are physically approximated together in order to close the regurgitant gap. Currently, the only FDA-approved TEER device is the MitraClip system (Abbott Inc.). First approved in 2013 for degenerative MR (DMR) and later in 2019 for functional MR (FMR), the current G4 system, released in 2020, features 4 differently sized devices that enable clinicians to tailor solutions to each patient and address a wide variety of anatomical and functional presentations of MR.

However, actual TEER clinical experiences remain mixed. For example, the EVEREST clinical trial compared TEER against surgical repair or replacement patients with mostly severe DMR and found that TEER was safer. However, TEER was less effective than surgery with respect to MR recurrence and the need for re-operation [6, 8, 9]. In 2018, the MITRA-FR and COAPT studies compared treatment with MitraClip plus guideline-directed medical therapy (GDMT) versus GDMT alone in relatively similar cohorts of patients with severe FMR [10, 11]. While the COAPT study found that TEER procedures had a beneficial effect on mortality and optimization, MITRA-FR found no such difference between the two groups. In addition, COAPT trial showed that death from any cause at 5-years is 57.6%. In an effort to empirically improve long-term outcomes, a number of guidelines have been developed to stratify patients based on clinical predictors of positive outcomes [3, 12, 13]. However, these guidelines tend to exclude a significant proportion of patients [14], and MR recurrence rates (defined as MR $\geq$ 2+) at 1-year reported in the literature continue to rise as high as 33% [15–18]. In summary, the principal challenges that impede the optimal clinical use of MV TEER, and in particular its durability, include (1) unclear patient selection, (2) heuristic clip placement, and (3) unpredictable long-term outcomes [3].

An additional limitation of previous studies is that they have not adequately addressed the long-term effects of TEER on the MV leaflet itself, as well as the impact of any observed remodeling on the durability of the repair. We and others have previously shown that the MV undergoes substantial changes in multiscale-level growth and remodeling as a direct consequence of ventricular dilatation and subsequent leaflet tethering [19–24]. Beyond a simple increase in MV leaflet area [25–27], prolonged leaflet tethering consistently induced MV leaflet thickness, which in turn stiffens the leaflet. It is thought that this is due to upregulation of collagen synthesis and fibrosis [24, 28–30]. These studies suggest that post-repair remodeling is a significant factor in determining MV repair durability.

Computational simulations can be of particular utility to improve MV TEER outcomes, as they can enable preoperative patient-specific optimization from standard-of-care in vivo images. Since the FDA approval of the MitraClip, many groups have developed in silico simulations of the TEER procedure. However, many of these studies have simplified the action of the clip device using connectors, stiff springs, or rigid plates [31–41], or developed the MV models using CT or magnetic resonance imaging, which is not the standard-of-care imaging of choice for MR and TEER [42–47]. We and others have developed patient-specific simulations using 3D transesophageal echocardiographic imaging with full 3D models of the TEER devices [48, 49]. Nevertheless, to our knowledge no image-based, patient-specific computational studies of MV function over time following TEER have been conducted.

We recently applied our in vivo MV geometry recovery method [50] to compute pre- and post-TEER MV leaflet strains in 10 patients [48]. Interestingly, despite substantial variations in the MV pre-operative state and in the clip configurations, TEER induced significant but focal increases in radial strain in the MV A2, consistent with the clip placement. However, longer-term consequences of the TEER procedure remain unclear. In related *in vivo* image-based and *in vitro* mechanical studies, we have shown that the MV undergoes major changes in both geometry and deformation, particularly a marked loss of anisotropy due to radial stiffening [19, 21]. We also demonstrated that these observed changes were entirely permanent, and were thus a form a *plastic* deformation. To evaluate this hypothesis we developed a soft tissue plasticity modeling framework in an ovine infarction model. We were able to able to *predict* the MV geometry and function 8-weeks after myocardial infarction [51].

These studies suggest that a plastic-like mechanism may occur in the MV post-TEER. Specifically, we hypothesized that the focal MV leaflet stresses imposed by the TEER device will induce plasticity-based remodeling responses. To assess this hypotheses, we applied our in vivo MV geometry recovery method to compute pre-, post-, and three month followup MV TEER leaflet strains in five patients. We first acquired standard of care 3D transesophageal echocardiographic (3D TEE) images at the pre- and post-operative time points. Next, given that functional instability has been observed clinically at 3 months [52–54], we acquired a final set of 3D TEE images at this followup timepoint. By computing end-diastolic MV leaflet strains at each time point, we

will be able to isolate the presence of plasticity that developed post-TEER. This study represents the first clinical-imaging based, longitudinal in silico study of MV TEER in humans.

2. METHODS

2.1. Summary of approach

In the present study we evaluated how the human MV initially adapts to the presence of the TEER device, then detected if the MV leaflets deform plastically after three months. Specifically, starting with the MV leaflets in the pre-operative end-diastolic state, we evaluated their geometries at the (1) pre-operative systolic (2) post-operative end-diastolic (3) post-operative end-systolic (4) follow-up end-diastolic and (5) follow-up end-systolic states. For the post-operative and follow-up simulations, previously described 3D models of the MitraClip [48] were directly implemented on the MV leaflets, with the number and type corresponding to each patient, and the clip positions on the leaflets were matched to the echo-derived segmentations. First, we computed the systolic closure strains referenced to the respective end-diastolic state for each time point. Next, we also computed teh diastolic strains: as the end-diastolic states are not subject to systolic pressurization, diastolic strains provide a measure of plastic deformation. Finally, we computed correlations of the strain fields in the same patient versus across patients to determine the extent to which the follow-up state is directed by the pre-operative state.

2.2. Patient enrollment and imaging

We obtained approval from the Institutional Review Board at the University of Texas at Austin to acquire additional 3D transesophageal echocardiographic (TEE) images at 3-months following the TEER procedure in consented patients, in addition to the usual, standard-of-care intraoperative TEE images at the time of the procedure. Thus, we were able to obtain longitudinal, 3D imaging at three separate time points for each patient: preoperative (immediately before device implantation), postoperative (immediately after implantation and release), and three months post-procedure. Based on our previous studies [51], we determined that four patients were necessary to detect the presence of plasticity at follow-up with a 95% confidence interval. Therefore, we aimed to recruit at least this many patients for our study. Full volume images were acquired using the Philips ie33 (Philips Medical, Andover, MA, USA) ultrasound system equipped with a 2–7 MHz X7-2t TEE matrix transducer. The scans were imported into Philips Ultrasound Workspace with an approximate isotropic resolution of 0.6-0.8 mm and exported as Cartesian DICOM files, then converted to the NIfTI format in ITK-SNAP.

2.2.1. Image segmentation

The pipeline for segmenting and meshing the MV geometry from clinical TEE images has been extensively detailed in [50]. Briefly, representative frames at end-diastole (ED) and end-systole (ES) were selected from all three image sets (preoperative, postoperative, and follow-up).

These frames were segmented using an interactive MATLAB tracing program. The annulus was first rotated to the short-axis view, and the geometric center of the MV orifice was translated to the intersection of the intercommissural and septolateral planes. Several septolateral cross-sections spanning the full intercommissural diameter of the MV orifice were made at 1 mm intervals, and at each cross-section, the anterior and posterior leaflets were traced as separate midsurfaces from the annulus to the free edge. Each image was segmented to include as much of the commissures as possible while using only identifiable leaflet tissue. The points in each traced curve were connected using shape-preserving piecewise cubic spline interpolation. Each curve was then rediscretized into segments of equal arc length and developed into a mesh using 2D Delaunay triangulation, Poisson-disk sampling, ball-pivoting reconstruction, and Taubin smoothing algorithms. Small regional gaps at the commissures were interpolated when necessary. This procedure resulted in meshes with uniform, unstructured nodal distributions, nodes spaced approximately 1 mm apart, and approximately 2000 elements per MV mesh, which were defined as 3-node triangular shell elements (S3) in Abaqus/Explicit (Dassault Systèmes). For the post-operative and follow-up ED and ES segmentations where the MitraClip device is present, it was not possible to reliably distinguish the length of the leaflet grasped within the device. Therefore, we manually traced the leaflets until the superior border of the device and used the geometry recovery technique described below to reconstruct this missing length [48]. Furthermore, this method of segmentation leaves an opening roughly circumscribing the clip device(s): we used the center of these openings to measure the position of the clip and define its displacement during the simulation.

2.2.2. Computation of MV leaflet systolic and diastolic strains.

A critical limitation of all direct 3D TEE methods is that the full coaptation zone of the MV cannot be directly visualized, as the two leaflets cannot be distinguished in this region. Thus, direct and accurate computation of leaflet geometry and strain mismatch cannot be determined [55]. Additionally, as the end-diastolic (ED) and end-systolic (ES) states are segmented independently, there is no material point correspondence between the resulting meshes at each time point. Moreover, in TEER cases the leaflet tissue grasped in the device cannot be reliably visualized or segmented, leaving gaps in the post-operative and follow-up segmentations.

To address these issues, we applied a previously described and extensively validated in vivo MV geometry recovery technique to recover of the full leaflet geometry that also ensures material point correspondence between all the meshes for each patient (Fig. 1) [21, 48, 50, 55, 56]. In brief, all geometry recovery shape-matching simulations were performed using Abaqus/Explicit 6.14. Frictionless self-contact of the MV leaflet surface was enforced with a penalty contact method, and the triangulated leaflet mesh was defined with isoparametric S3 shell elements with a homogenous leaflet thickness of 1.5 mm. We utilized a nearly incompressible isotropic non-linear constitutive model for the MV leaflet tissue [50]. It is important to note that the form of this con-

stitutive model allows for strain-induced mechanical anisotropy that can occur in the MV leaflet [57]. The specialized constitutive model was implemented in an Abaqus/Explicit subroutine (VUMAT) for FE simulations. Though this relation has been shown to sufficiently model MV leaflet tissue, it is important to note that tissue elasticity is used only to *regularize* the morphing process of the MV geometry, as the present technique does not require precise knowledge of MV leaflet tissue mechanical properties.

The boundary and loading conditions used in the simulations have been presented previously [50]. Briefly, annular displacements were determined using the geometries extracted from the open and closed MV states in each pre-operative image. We assumed a uniform percent change across the entire circumference of the annulus [58]. A uniform, physiological pressure of 100 mmHg was applied to the ventricular surface of the MV leaflets, and a downward chordal mimicking force (CMF) was applied to the free edge. Finally, we penalized any mismatch between the simulated and target (i.e. imaged) closed shapes of the leaflets using a local corrective pressure field (LCPF), which was at any instance and location linearly proportional to the shortest distance between the MV mesh and the target closed MV medial surface. We first defined a 3D spatial domain encompassing the entire target closed MV. Then, we discretized this domain with an isotopic 0.5 mm resolution to obtain a set of query points from which we calculated the point-to-surface distance vector field to the target closed MV geometry. To allow for fast real-time analytic evaluation of the LCPF during the FE simulation, we reconstructed each component of this distance field using a 3D cosine series. The LCPF was specified increment-wise as a nonuniform distributed pressure using the Abaqus/Explicit Fortran subroutine VDLOAD.

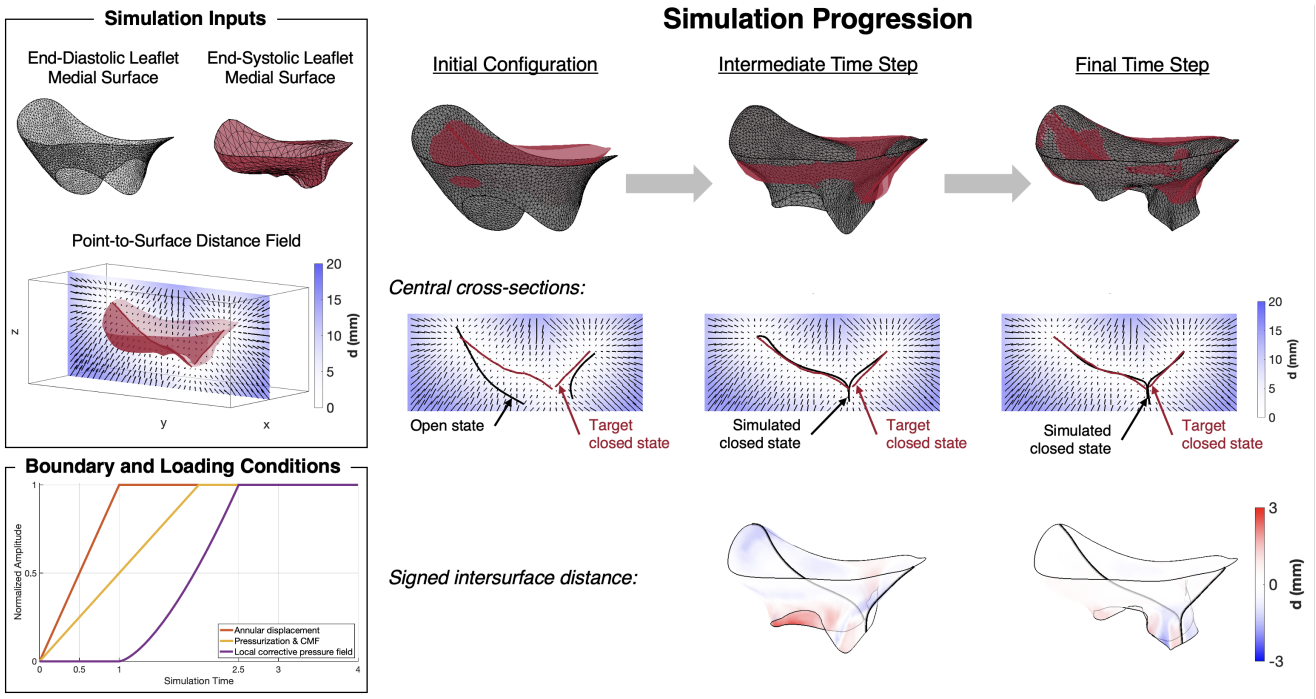

Figure 1: An overview of the in-vivo geometry MV recovery pipeline. First, MV leaflet medial surfaces were segmented from 3D echocardiographic images at ED and ES. Then, the 3D distance field enclosing the end-systolic medial surface to the nodes on the surface is computed. Annular displacement is applied as a boundary condition, and a physiological pressure of 100 mmHg is applied on the ventricular side and a chordal mimicking force is applied on the free edge nodes. Once the MV has initially closed, a local corrective pressure field, proportional to the point-to-surface distance field, is applied on the atrial side of the leaflets to enforce the end-systolic shape. The progression of the simulation from the open state to the final closed state is shown, first in cross-sections superimposed over the local corrective pressure field; then in 3D (simulated mesh in grey, target mesh in red); and finally in 3D with the signed intersurface error plotted. See text for complete details. Legend: MV: mitral valve; ED: end-diastole; ES: end-systole

2.3. Post-TEER simulations

The post-operative and follow-up TEER simulations followed a similar in vivo geometry recovery protocol as above. The key difference was the addition of appropriate 3D models of the MitraClip positioned as described in Section 2.2.1. We have previously described the integration of the TEER procedure with the pre-operative simulation in [48]. To summarize, the movement and grasping of the clips occurred in parallel to the closure of the MV leaflets in a four-step Abaqus sequence. In Step 1, the MV leaflet portion of the simulation has not yet begun, and the clips are simply moved downward to prevent interference with the leaflets during closure. In Step 2, the boundary, pressurization, and CMF conditions are activated on the MV leaflets to begin leaflet closure, while the clips move back up and to their echo-dictated positions as defined previously. From this step onwards, a hard contact pressure-overclosure relationship is enforced on all exterior surfaces to prevent intersection of the leaflets and clip structures. Next, once the ventricular pressure reaches 50 mmHg, the local corrective pressure field is activated on the atrial surface of the MV leaflets and the clips remain in their final positions. In the last step, the clip arms rotate 60 degrees towards the grippers and grasp the leaflets. Rough friction

contact with no slippage or separation was assigned to the inward-facing surfaces of the grippers and arms to prevent the MV leaflets from sliding out of the clip grasp (Fig. 2).

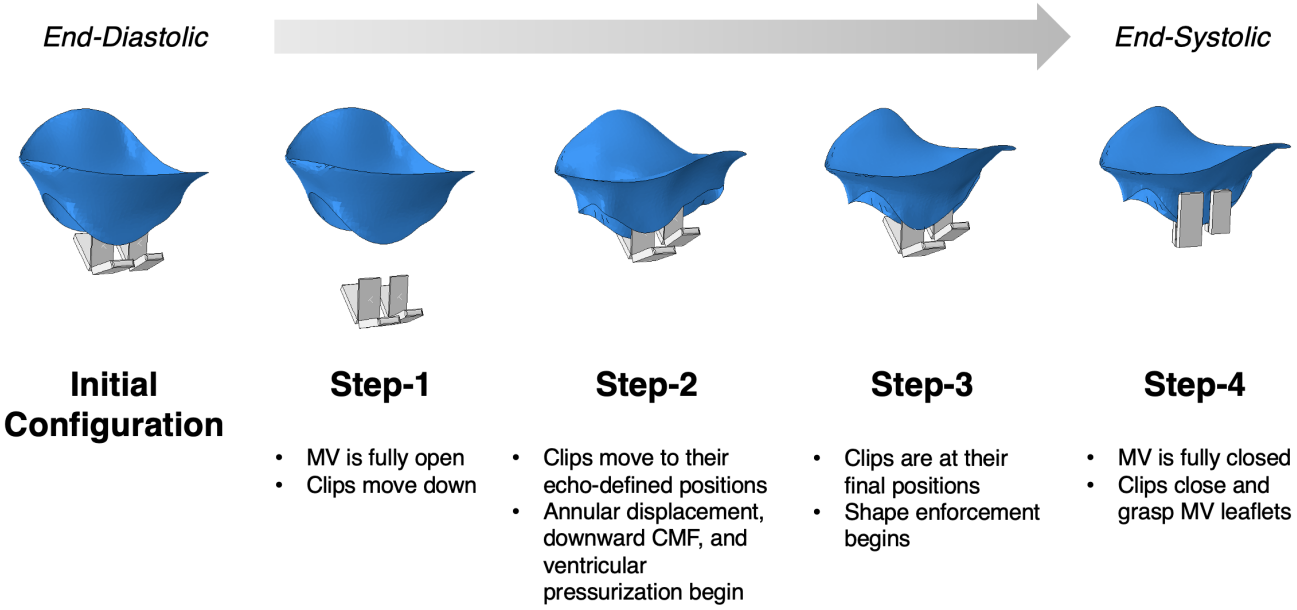

Figure 2: The step sequence of the post-operative GOsimulation with clip actuation. As in the pre-operative simulation, the sequence begins at the end-diastole and progresses towards end-systole. The clips move to their final, echo-dictated positions as morphing of the open MV mesh to match the closed shape occurs. When the MV has fully closed and is in its echo-derived systolic shape, the clip arms close onto and grip the MV leaflets. MV: mitral valve

For this study, we also applied the in vivo geometry recovery technique to simulate the post-TEER ED states. The purpose of this step–rather than using the direct segmentation–was first to apply the 3D models of the clips while also enforcing an accurate final geometry and also to ensure material point correspondence between all meshes for each patient. However, with the ED geometries, we experienced an additional challenge, namely over-closure in the openings of the double orifice. In the systolic state, we do not have this issue, as the leaflet-to-leaflet contact in the coaptation zone prevents over-closure. In contrast, the leaflets in the ED state are naturally not in contact in the orifice areas, and the leaflet edge can overshoot its intended position, resulting in an incorrect approximation of the leaflets. Therefore, we incorporated a synthetic barrier with the segmented target meshes (in both ED and ES, for consistency) in order to prevent this issue. As the LCPF enforces this barrier, the simulated mesh cannot overstep this boundary and cross into the orifice area. With this method, we were able to accurately reconstruct the ED-state meshes such that the surface-to-surface error against the segmentated surfaces was less than 0.6 mm (below voxel resolution) in all cases.

2.4. Simulation kinematic analyses.

To compute the in-surface strains from a given reference to current configuration, we defined the reference nodal positions as $\mathbf{X}$ and the current nodal positions as $\mathbf{x}$. Next, we apply a

rotation matrix $\mathbf{R}$ to $\mathbf{X}$ to align the local material directions $\langle \hat{\mathbf{r}}, \hat{\mathbf{c}}, \hat{\mathbf{n}} \rangle$ with the spatial directions $\langle \hat{\mathbf{e_x}}, \hat{\mathbf{e_y}}, -\hat{\mathbf{e_z}} \rangle$. For the current configuration, as the local material directions may no longer be mutually orthogonal due to the deformation of the element, they are recomputed in the current state, and again applied as a rotation matrix to $\mathbf{x}$. Using these aligned nodes, we define the displacement $\mathbf{u}$ as:

$$\mathbf{u} = \mathbf{x} - \mathbf{X} \tag{1}$$

and the deformation gradient $\mathbf{F}$ as:

$$\mathbf{F} = \mathbf{I} + \frac{\partial \mathbf{u}}{\partial \mathbf{X}} \tag{2}$$

The S3 shell elements provided in ABAQUS/Explicit are linear, triangular isoparametric elements; using the standard shape functions for this type of element and Eqns. 1 and 2, the deformation gradient can be easily computed. From $\mathbf{F}$, we then computed the right Cauchy-Green deformation tensor $\mathbf{C}$ using

$$\mathbf{C} = \mathbf{F}^T \mathbf{F},$$

where due to incompressiblity $C_{33} = \frac{1}{det \mathbf{C_{2D}}}$. Next, using the right stretch tensor $\mathbf{U} = \sqrt{\mathbf{C}}$, we computed the principal stretches and directions.

To determine the presence of plasticity in the MV leaflets post-TEER, we first defined the following numbering scheme for each MV state considered, number 0 to 5 (Figure 3). Here, the even numbers represent the ED state and the odd numbers represent the ES states. For this study, we define plasticity, $\mathbf{F^p}$, as any additional deformation from the post-ED state to the followup-ED state. As both ED states are not under systolic pressurization and both states are from the same patient and therefore have the same TEER configuration, any observed "deformation" must be due to underlying plastic processes over time. In this numbering scheme, this would represent deformation from state 2 to state 4, so that $\mathbf{F}^p = {}^4_2\mathbf{F}$.

In order to compute the plasticity deformation gradient, we utilized the multiplicative decomposition of the total deformation gradient tensor $\mathbf{F}$ into its elastic and plastic components [59, 60]:

$$\mathbf{F} = \mathbf{F^e F^p} \tag{3}$$

The total deformation gradient $\mathbf{F}$ that involves both the plastic deformation from post-ED to followup-ED, as well as the corresponding elastic deformation due to systolic pressurization from followup-ED to followup-ES is the deformation from post-ED to followup-ES. In terms of our numbering scheme introduced above, Eqn. 3 becomes

$${}^5_2\mathbf{F} = {}^5_4\mathbf{F}\ {}^4_2\mathbf{F} \tag{4}$$

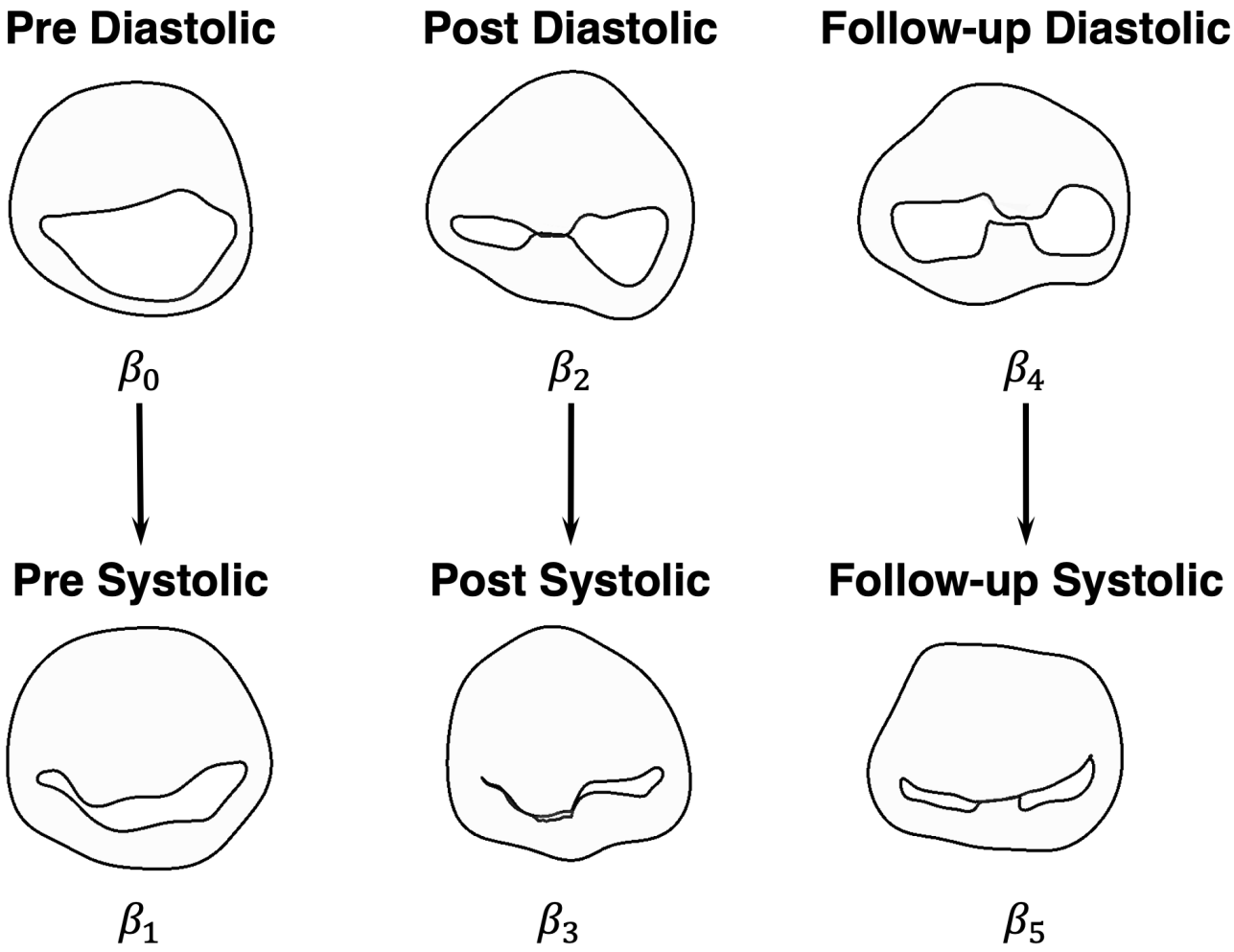

Figure 3: A representative MV shown in the six time steps (β_i) analyzed in this study, namely the end-diastolic and end-systolic states in the cardiac cycle from imaging done at the pre-operative, post-operative, and follow-up (3-months) time points. MV: mitral valve.

2.5. Statistical analysis

To assess the global strain fields by Carpentier segment (Fig. 4) and to evaluate the relationship between the pre- and post-operative strain fields, the computed strain fields were re-expressed in a 2D parametric space that allowed for direct correspondence of material points between meshes. Using these 2D representations of the circumferential and radial strain fields, we calculated the 2D correlation coefficients between the pre- and post-operative systolic strain fields of the same patient (Intra) and paired across patients (Inter). We also repeated this analysis for the pre-operative/follow-up strain fields and the post-operative/follow-up strain fields. All correlations were computed for the circumferential, radial, and first and second principal directions. The 2D correlation coefficient R is defined as

$$R = \frac{\sum_i \sum_j (A_{ij} - \bar{A})(B_{ij} - \bar{B})}{\sqrt{(\sum_i \sum_j (A_{ij} - \bar{A})^2)(\sum_i \sum_j (B_{ij} - \bar{B})^2)}} \tag{5}$$

where $\mathbf{A}$ and $\mathbf{B}$ are the two strain tensor fields being compared. Two-tailed Student's t-tests were used to compare 2D correlation coefficients and Carpentier segment strain averages and one-sample Student's t-tests were used to assess the difference of these values from zero, with a p-value of less than 0.05 considered statistically significant.

2.6. Assessment of left ventricular dimensional stability

We explored the possibility that any observed MV leaflet tissue plasticity could be driven by continued ventricular remodeling, resulting in annular or ventricular dilatation. First, we computed the anteroposterior and intercommissural dimensions for each patient at the three timepoints. We found the annulus points with x-values nearest to zero (anteroposterior) and y-values nearest to zero (intercommissural) and computed the magnitude of the distance between each pair of points (Fig. 4). Next, we calculated the annular perimeter by summing the Euclidean norm of each 3D line segment connecting adjacent points on the annulus. Finally, we computed the end-diastolic MV leaflet area by summing the areas of each element on the ED-state mesh, as computed in Eqn. 6, where a, b, and c represent the vertices of a given triangular element:

$$A_{elem} = 0.5 * \|(b-a) \times (c-a)\| \tag{6}$$

In order to approximate any ventricular dilatation over time, we measured standard markers of LV size from transthoracic echocardiographic (TTE) images taken preoperatively, at 30-day followup, and 1-year followup, as per ASE guidelines [61]. We were able to quantify LV end-systolic dimension (LVESD), LV end-diastolic dimension (LVEDD), LV end-systolic volume (LVESV), and LV end-diastolic volume (LVEDV). Though we have data for all five patients at the preoperative and 30-day timepoints, one year has not yet passed for two of the patients (MV4 and MV5), so the data at this timepoint is incomplete. As these data were of the repeated measures form, we used paired, one-tailed Student's t-tests to assess the difference of the geometric measures from each other across time. However, for the difference in LV dimensions from 30-days to 1-year, as we are missing data from 2 patients at 1-year, these cannot be treated as repeated measures, and a one-tailed standard Student's t-test was used.

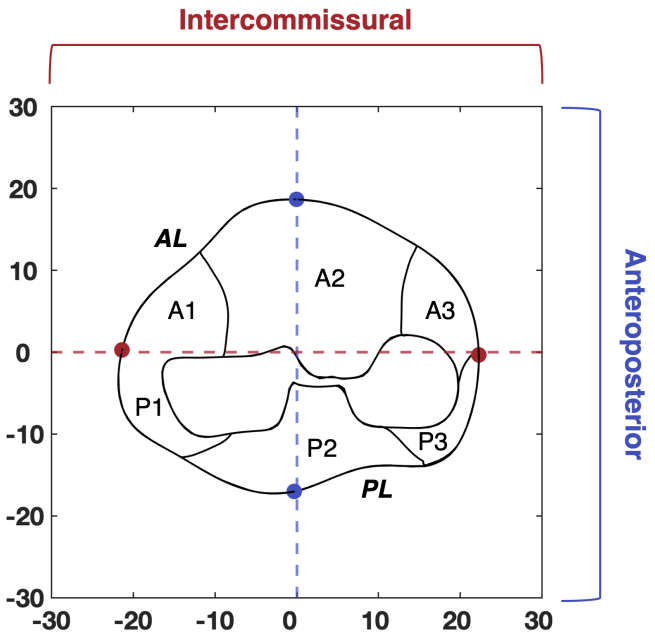

Figure 4: Definition of anteroposterior and intercommisural dimensions and Carpentier segments. The anteroposterior dimension was defined as the distance between the two annular points whose x-value was nearest zero (highlighted in blue). The intercommisural dimension was defined as the distance between the two annular points whose y-value was nearest zero (highlighted in red).

3. RESULTS

3.1. Patient characteristics

We recruited a total of five patients that spanned a wide range of MR types, including degenerative, functional (both ischemic and non-ischemic), and mixed etiologies (Table 1). Moreover, almost all patients received different MitraClip device configurations; though both the first and fourth patients received the NTW device, it was placed in A2/P2 and A1/P1 segments, respectively. Therefore, even this modest cohort of patients highlights the vast heterogeneity of clinical presentations typical of this disease.

Patient information	MV1	MV2	MV3	MV4	MV5
Age	79	66	71	76	70
Race	White	White	Hispanic	Hispanic	White
Sex	F	F	F	M	F
MR etiology	Mixed	FMR	FMR	DMR	FMR
Clips	NTW	XTW, NT	XTW, NT	NTW	XTW

Table 1: Relevant patient demographics, MR etiology, and clip configurations used in the TEER procedure. FMR: functional mitral regurgitaton; DMR: degenerative mitral regurgitation

MR severity	MV1	MV2	MV3	MV4	MV5
Post-procedure	Moderate	Mild-moderate	Mild	Mild	Mild
30 days (TTE)	Moderate-severe	Mild-moderate	Mild	Mild	Mild-moderate
3 months (TEE)	Moderate-severe	Moderate	Mild-moderate	Mild-moderate	Mild-moderate
1 year (TTE)	Moderate-severe	Moderate	Mild-moderate	Pending	Pending

Table 2: Post-intervention MR severity over time.

3.2. *Variability in pre- and postoperative deformation*

As in our previous TEER study [48], we observed substantial variation in the preoperative deformation of the patients' MVs prior to TEER intervention. As expected, the circumferential direction tends to be more compressive, while the radial is more extensive (Figs. 5, 6). This result also agrees with our previous findings regarding ischemic MR patients before treatment with undersized ring annuloplasty [56]. However, beyond these general trends, there are no obvious patterns in preoperative systolic deformation across the patients. Importantly, these results once again underscore the heterogeneity of the MR patient population, and further emphasize the need for a robust, patient-specific approach to treatment.

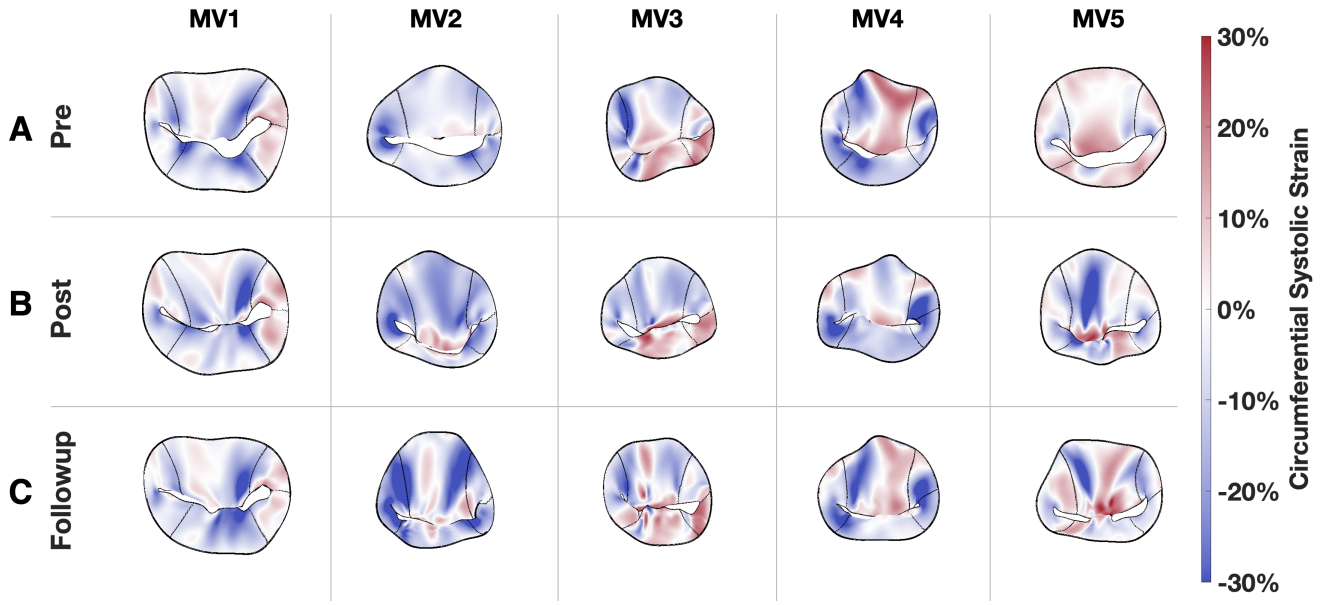

Figure 5: Circumferential systolic strain for each patient preoperatively, post-TEER and at the 3-month followup timepoint. The strain patterns are highly variable, though generally compressive.

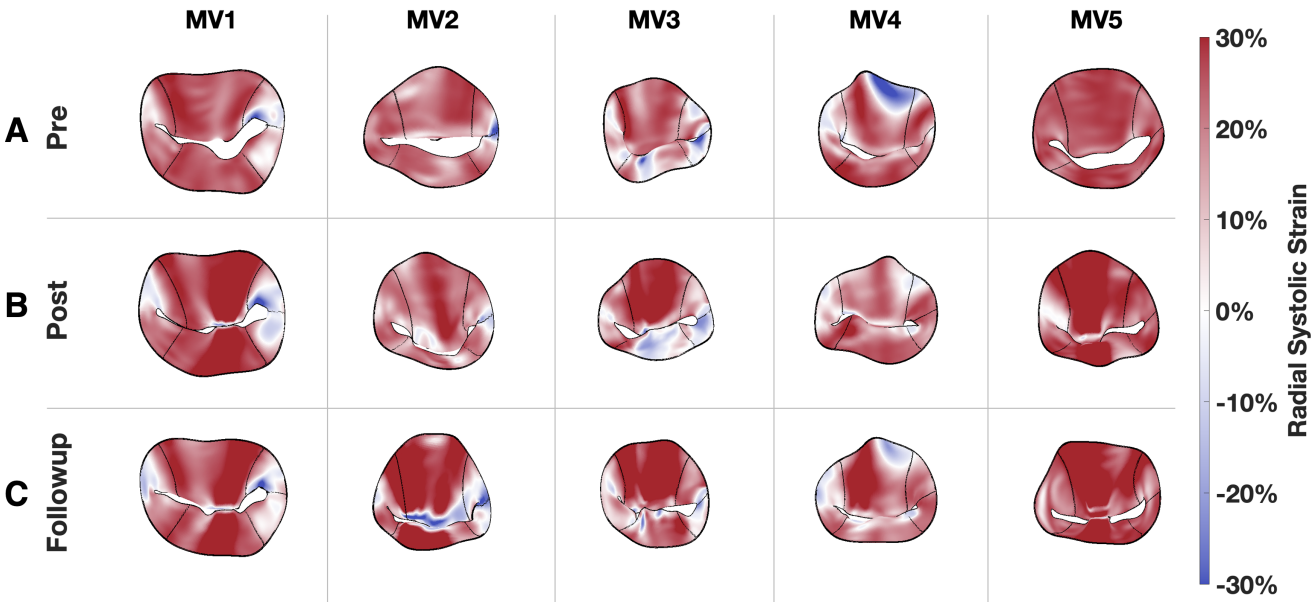

Figure 6: Radial systolic strain for each patient preoperatively, post-TEER and at the 3-month followup timepoint. The strain in this direction is mainly extensive, with highly localized "hotspots" concentrated to the clip positions. Despite these similarities across the patients, the strain patterns are highly heterogeneous and differ markedly from valve to valve.

Following the TEER procedure we found a general increase in local radial strain corresponding to the location of clip placement (Fig. 6). When averaged together, we found no statistical significance in the difference between preoperative and postoperative strain by segment. However, this can be attributed to the fact that the patients received different clip configurations in different regions of the MVs, which would not necessarily lend itself to pooling by segment. Interestingly, when we referenced the systolic strain to the current end-diastolic configuration, we found marked stiffening of the leaflets in the radial direction post-intervention (Fig. 7). In contrast, when referenced to the preoperative ED state, the radial strains remain fairly consistent. This result demonstrates the major restrictive impact of TEER on the function of the native MV.

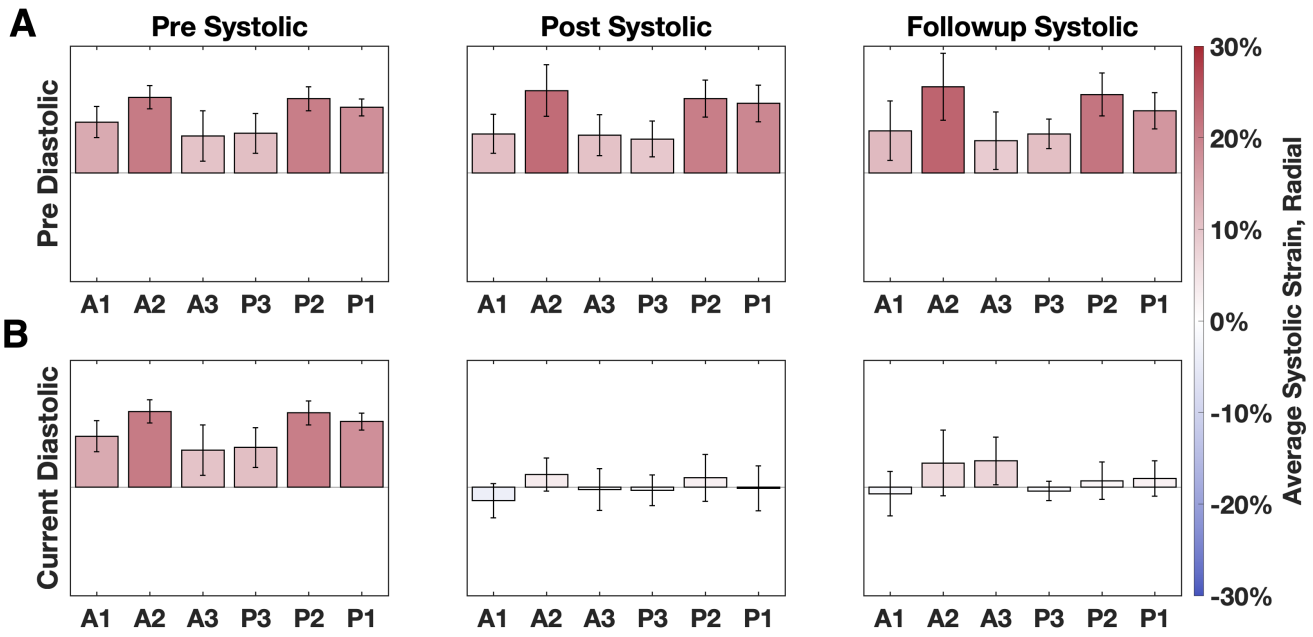

Figure 7: Radial systolic strain averaged across all patients at the preoperative, postoperative, and followup time points, referenced to A: the preoperative end-diastolic configuration and B: the respective current diastolic configuration. (Note that for the preoperative systolic state, the preoperative ED state is equivalent to the current ED state.) There is a major stiffening observed post-TEER when the deformation is referenced to the current ED configuration, which underscores the degree to which TEER restricts MV deformation.

3.3. Evidence of plastic deformation following TEER at three months post-operation

Importantly, we found significant evidence of continued plastic deformation in the patient MVs at three months post-TEER. In the circumferential and radial directions, the patterns are highly complex and heterogeneous, with compressive and extensive regions juxtaposing each other across the valve tissue. In contrast, in the principal directions, the patterns are much clearer. The first principal stretch is generally extensive for all the patients, and the regions of highest principal stretch are concentrated in the regions of the clip(s) (Fig. 8). Similarly, the first principal directions also all converge onto the position of the clip(s), strongly supporting our hypothesis that the clip is the cause of the observed plastic deformation. The second principal stretches are on the whole more compressive, though certain patients have compact extensional zones. Again, any regions of relatively high stretch, either compressive or extensive, seem to be concentrated along the positions of the clip(s). When averaged by Carpentier segment, we found 10-20% plastic strain in all segments and that the magnitude of plastic strain in both principal directions was significantly different from zero in each segment ($p < 0.05$; Fig. 9). The highest incidence of plasticity in the first principal direction was observed in the A2 and P2 segments, likely due to the fact that every patient had at least one clip placed in this central location. In the second principal direction, the plastic strains tend to be more uniform, though the P3 segment demonstrated significantly lower plastic strain in this direction when compared to A2 or P2.

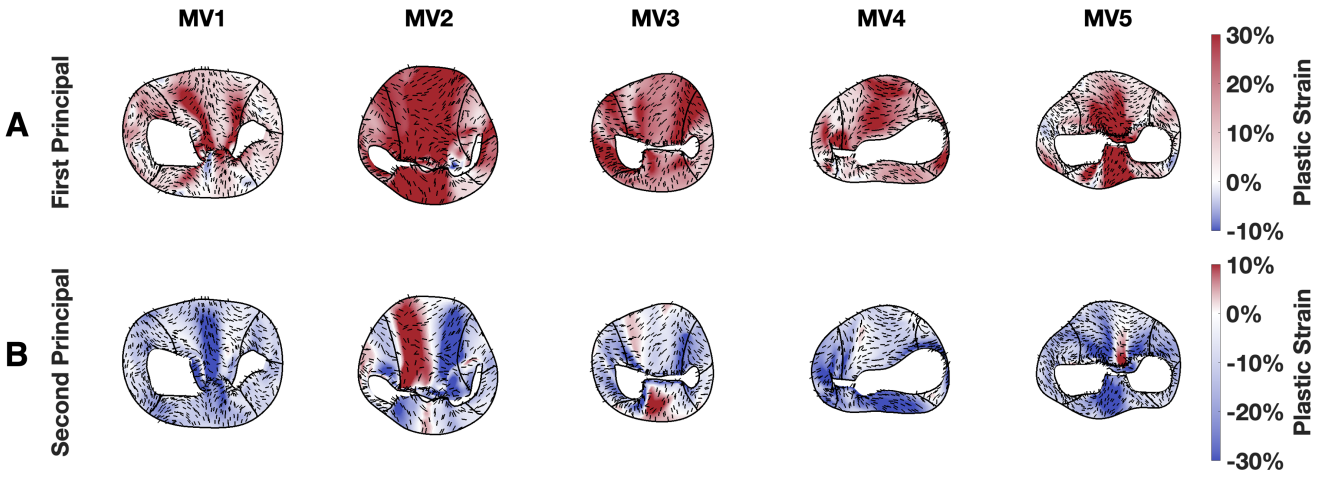

Figure 8: Patient-specific end-diastolic MV geometries at 3-month followup, plotted with the magnitude of first and second principal plastic strain magnitudes and directions. Carpentier segment boundaries are also plotted. The plasticity in the first principal direction is concentrated in the region of clip(s) for each patient, and is highly extensive. Similarly, the first principal directions converge onto the position of the clip in all five patients. The magnitudes of the second principal strain also correspond to the clip positions and are generally compressive, though some of the valves also demonstrate zones of extensive strain in these regions.

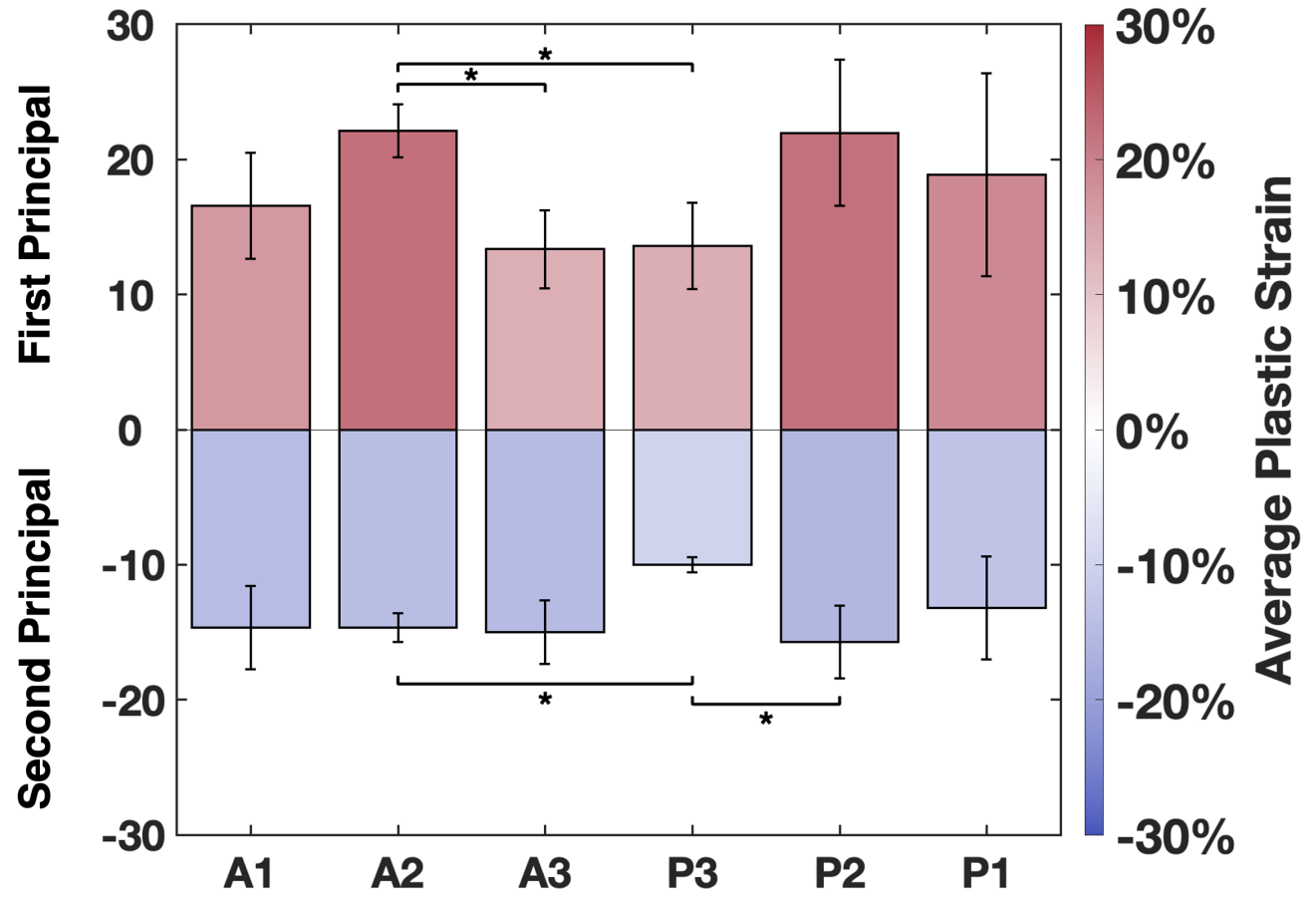

Figure 9: The plastic strain, averaged across all patients, in each Carpentier segment in the first and second principal directions. All strains are significantly different from zero ($p < 0.05$). The largest changes are in A2 and P2 in the first principal direction as expected, as this is where every patient had at least one clip placed.

3.4. *Dimensional changes*

The analysis of the MV geometries revealed limited significant differences from the pre- to post-TEER time points as expected, but importantly no changes from post-TEER to the three month followup. Specifically, we found that TEER induced an immediate, significant reduction in the annnular anteroposterior (AP) dimension, which likely corresponds to the grasping axis perpendicular to the commissural line (Fig. 10A). This finding corresponds to observations in the clinical literature [62, 63]. There was also a significant increase in ED leaflet area immediately post-TEER, likely due to TEER device(s) stretching the leaflets into the double orifice configurations. However, we did not observe any significant changes in annular length or intercommissural dimension. Importantly, we did not observe any significant changes across any of these geometric measurements from immediately post-TEER to the 3-month followup timepoint (Fig. 10B). This finding suggests that the plasticity observed in Section 3.3 cannot be attributed to continued annular dilatation. Similarly, the LV measurements do not reveal any significant increases from the 30-day to 1-year timepoints 11. Therefore, the observed plasticity does not appear to be driven by left ventricular dilatation either.

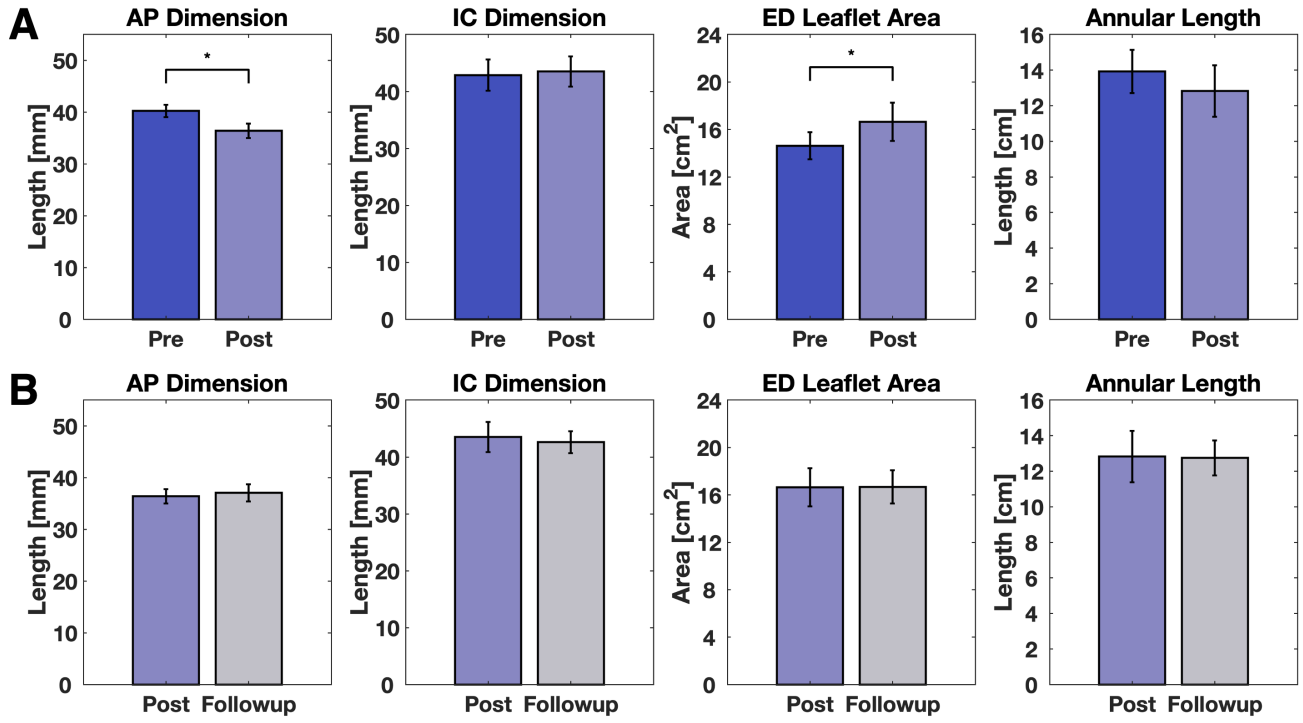

Figure 10: Changes in annular dimensions, end-diastolic leaflet area, and annular length over time. A: TEER induces a significant decrease in anteroposterior dimension and an increase in end-diastolic leaflet area, but no changes were observed in intercommissural dimension or annular length. B: No significant differences were observed from immediately post-TEER to 3-month followup in any of the measured dimensional metrics. Bars represent mean +/- standard error. AP: anteroposterior; IC: intercommisssural; ED: end-diastolic

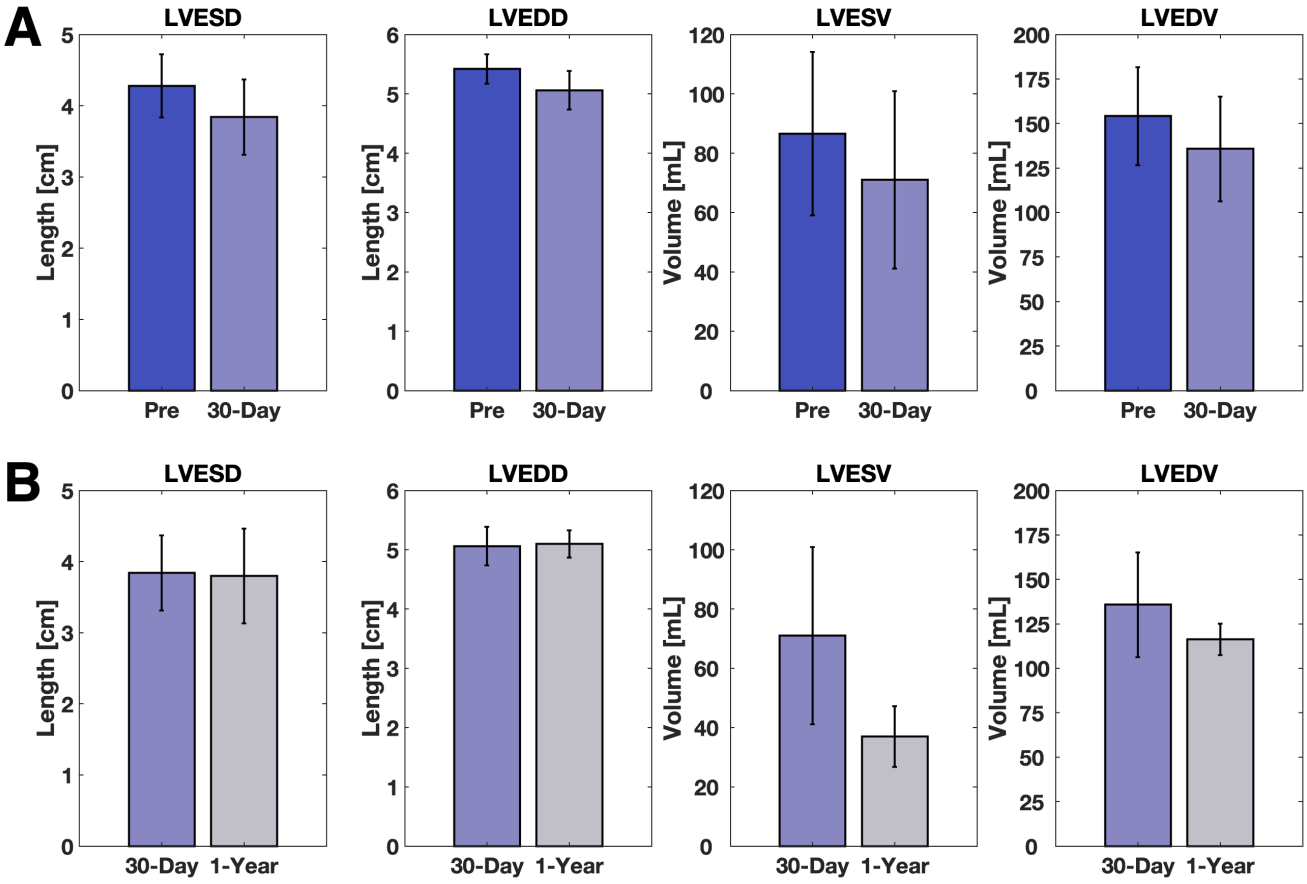

Figure 11: Changes in left ventricular dimensions before TEER, 30-days after TEER, and 1-year after TEER. A: No significant changes in LV dimensions were observed from preop to 30-days, except a significant decrease in LVEDD. B: No significant changes were observed in any of the measurements from 30-days to 1-year, indicating that the ventricle did not continue to dilate in these patients post-repair. Bars represent mean +/- standard error, and the 1-year timepoint includes only the 3 patients who have passed the 1-year followup timepoint. LVESD: left-ventricular end-systolic dimension; LVEDD: left-ventricular end-diastolic dimension; LVESV: left-ventricular end-systolic volume; LVEDV: left-ventricular end-diastolic volume.

3.5. Correlations in kinematic behaviors

We found that the self-paired pre/post systolic stretch fields correlated better than the inter-patient pairs (Fig. 12A, $p < 0.05$). This was also true for the pre/followup systolic stretch fields and the post/followup systolic stretch fields (Fig. 12B and C, $p < 0.05$). Importantly, these results suggest that in spite of wide variability in deformation across the patients, the systolic deformation both immediately post-TEER and at 3-month follow up is related to, and therefore directed by, its initial preoperative state. Consequently, this lends strong support to the idea that the postoperative and even the three-month functional states can be *predicted* from preoperative data alone. Furthermore, we found that plasticity (i.e. deformation from the postoperative ED state to the followup ED state) was correlated with postoperative systolic stretch when referenced to the postoperative ED state (Fig. 13). This finding held for both material directions, as well as both principal directions. Again, this result suggests that the degree of plastic deformation in the patient MV could be *predicted* from clinical imaging data and a given clip configuration.

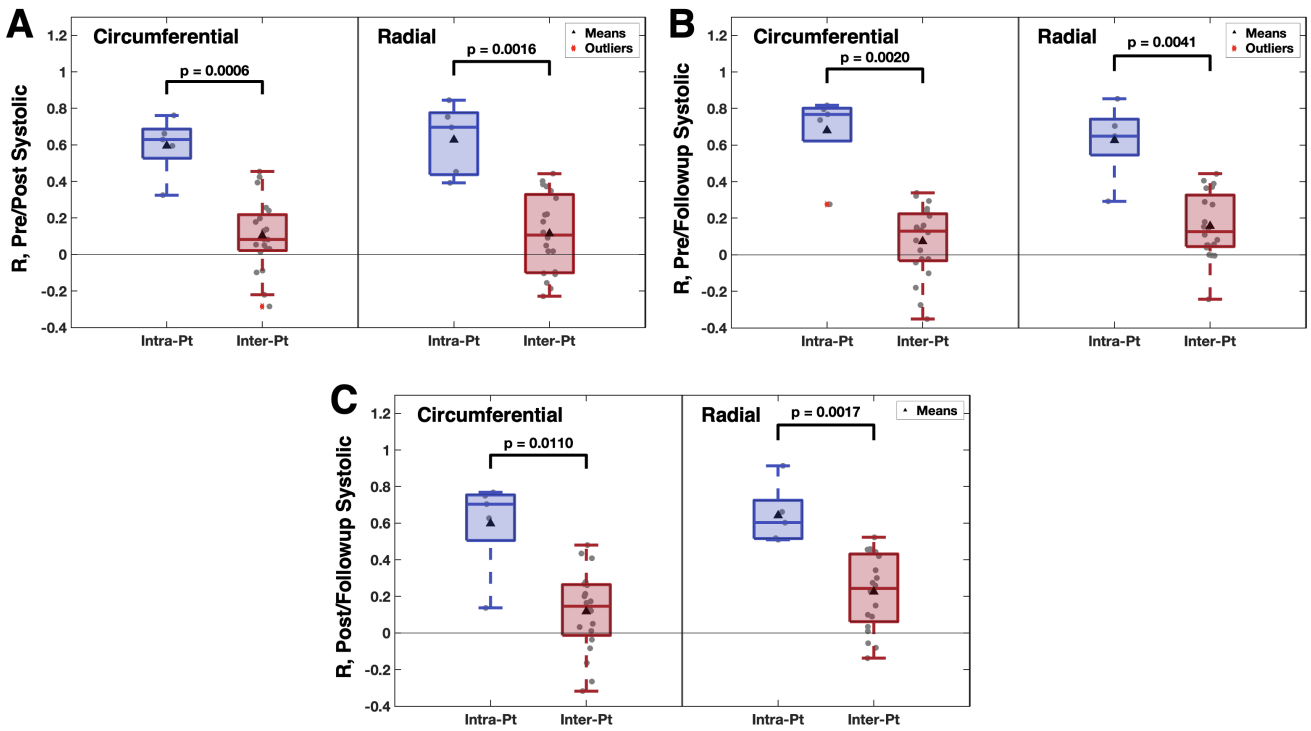

Figure 12: 2D correlations between systolic strain fields across time, both self-paired (Intra-Pt) and across patients (Inter-Pt). All systolic strain fields are referenced to the preoperative end-diastolic state. A: Pre-operative systolic strain correlated with post-operative systolic strain; B: Pre-operative systolic strain correlated with followup systolic strain; C: Post-operative systolic strain correlated with followup systolic strain. In all cases, for both the circumferential and radial material directions, the self-paired systolic strain fields were better correlated than the inter-patient pairs. These results indicate that postoperative deformation is directed by its respective preoperative state, and similarly followup deformation is directed by *both* its respective preoperative and postoperative states.

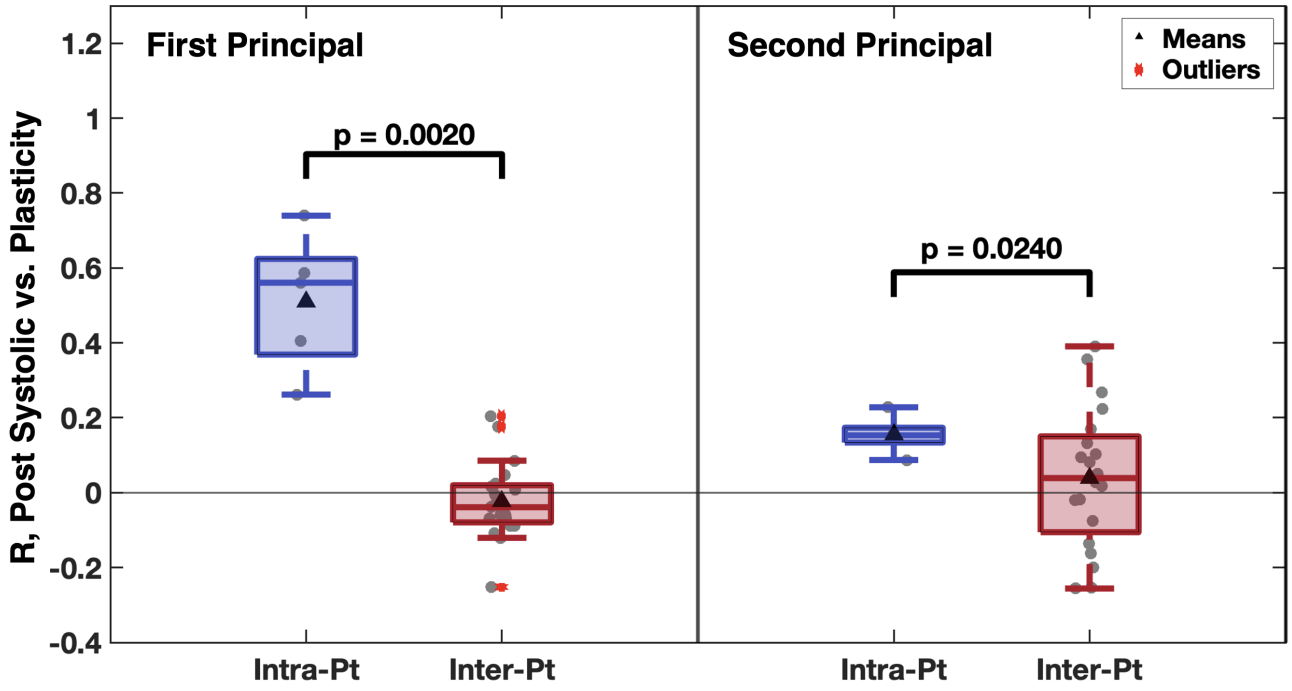

Figure 13: 2D correlations between the postoperative systolic strain (referenced to the *postoperative* end-diastolic state and plasticity, both self-paired (Intra-Pt) and across patients (Inter-Pt). In both the first and second principal directions, the self-paired correlation coefficient is significantly greater than that for random pairs across patients. This finding signifies that the postoperative systolic strain field, when referenced to its own postoperative end-diastolic state, directs the progression of plasticity until followup.

4. Discussion

4.1. Summary of findings

While the link between the focal stress induced by TEER and long-term functional deficits has been postulated [3, 64] and the capacity of the MV leaflets to remodel has been amply demonstrated [20, 21, 24, 26–29, 65, 66], these effects have not yet been explored in TEER patients. This longitudinal study is the first to quantify in vivo the onset of plasticity in human MV leaflets over time following transcatheter edge-to-edge repair. Specifically, this work brings to light the following observations regarding MV remodeling post-TEER:

1. There is significant evidence of plasticity present at 3-months following TEER, on the order of 10-20% strain.

2. The plastic strains are generally extensive in the first principal direction and compressive in the second principal direction.

3. Though the overall strain patterns vary considerably from patient to patient, in all patients the zone with highest magnitude of plasticity corresponds to the placement of the clip(s) (Fig. 8).

4. The first principal directions of this plastic strain converge onto the position of the clip(s), strongly indicating the role of the TEER device in inducing the observed plasticity (Fig. 8A).

5. The post-TEER systolic strain the MV experiences is dramatically reduced when referred to the *current end-diastolic state* (Fig. 7B). This functional deficit can likely be explained mainly by the restriction the clip places on the leaflet, as well as any plastic deformation, both of which can increase the stretch experienced by the leaflets in end-diastole and effectively lower the tissue's overall extensibility.

6. We observed no additional ventricular dilatation over the followup period, suggesting that continued ventricular remodeling is not a driver of the observed plasticity. The annular dimensions remain stable from immediately post-TEER to the 3-month followup (Fig. 10B). Similarly, there are no changes in LV dimension or volume from 30-days post-TEER to 1-year (Fig. 11B). Therefore, it is also unlikely that continued LV dilatation and an associated shift in papillary muscle positions are responsible for the observed plasticity.

7. The 3-month systolic strain fields are directly correlated to their corresponding pre-operative and post-operative systolic strain fields (Figs. 12B, C). These findings suggest that the pre-operative and post-operative functional states independently direct MV leaflet deformation at 3-months, which in turn suggests that *the followup functional state can be predicted from pre-operative data*.

8. Plasticity itself is directly correlated to the corresponding post-operative systolic strain *when referenced to the post-operative end-diastolic state* (Figs. 13). The fact that plasticity does not correlate with the pre-operative state directly is unsurprising, given that plastic response seems to be predominantly driven by the clips.

9. The degree of leaflet restriction imposed by the clip also appears to be integral to the development of plasticity, which may explain why it correlates to post-operative systolic deformation only when referenced to the current end-diastolic state.

This study also reinforces some important prior findings regarding the effect of TEER on MV geometry and function. First, we once again observed widespread heterogeneity of the pre-operative strain fields amongst the patients (Figs. 5A, 6A). Moreover, we also found that the clip induces a localized change in postoperative systolic strain; specifically in the radial direction, this change is markedly extensive (Fig. 6). Both of these findings echo those in our previous publication analyzing deformation patterns pre- and post-TEER [48]. Next, though we found no significant change in annular or LV dimensions from the given post-TEER to followup timepoints, we note that TEER induces a significant reduction in AP dimension, which can be

explained by the devices' approximating the leaflets along the AP axis, and an increase in end-diastolic leaflet area, likely due to the stretching experienced by the leaflets during filling in the highly restricted double-orifice configuration. Moreover, we found a significant decrease in LV end-diastolic dimension over 30-days post-TEER, suggesting that the LV is undergoing reverse remodeling. This observation is supported by almost all dimensional and volumetric measurements trending downwards (though not significantly) from pre-operative to 1-year follow-up. Finally, we also found that post-operative systolic deformation is directly correlated to each patient's corresponding pre-operative state, which aligns with our previous work [48], and once again suggests that the post-operative state is directed by and therefore can be predicted from pre-operative imaging alone. We have developed a computational pipeline to predicted the post-repair functional state from pre-operative clinical imaging in undersized ring annuloplasty patients [67], and work is ongoing to apply this approach to TEER patients.

4.2. Possible mechanisms driving MV plasticity

In our previous work, we have studied the onset and progression of ischemic MR following MI in sheep [19, 21]. An in vivo, image-based analysis of ovine MV geometry and deformation over 8 weeks post-MI revealed increasing radial diastolic stretches over time. As the diastolic state is effectively unloaded, this increase in "deformation" suggests that the MV leaflets increase in size relative to the pre-MI state due to the MI-induced change in boundary conditions [21]. To clarify whether this observation is driven mainly by biological mechanisms such as inflammation (discussed in detail in Section 4.3) or by mechanical distentions, we conducted another study involving in vitro structural examination of the same ovine MV tissue over time following MI [19]. At 8 weeks, the MV tissues showed a major loss of anisotropy marked by significant stiffening in the radial direction. Parameter estimation to a meso-scale structural constitutive model revealed that this stiffening could be attributed solely to a *permanent* reorientation and straightening of the collagen fiber network, and not to any intrinsic damage to the collagen itself. This finding suggests that, at least by the 8-week time point, the observed increase in MV leaflet area is largely due to permanent, mechanical distention of the leaflet tissue following continued annular and ventricular dilatation post-MI.

Given that the collagen modulus and mass fraction remain unchanged, and that the collagen fiber structure alone accounts for any changes in the tissue mechanical behavior, it appears that the observed plasticity results from changes in the ground matrix, rather than the collagen itself. This assumption was investigated with exogenously cross-linked bovine pericardial biomaterials (used in bioprosthetic heart valves) which substantially enlarge with in vivo operation [68]. In this work, a structural constitutive model based on the underlying scission-healing reaction of the GLUT crosslinked matrix was able to predict the function of the bioprosthetic heart valve tissue at 65 million cycles. Importantly, we then developed a similar model for the MV predicated on the key assumption that scission-healing in the MV tissue ground matrix drives the

permanent changes described above. This model was also able to predict post-MI geometry and function at 8 weeks with a high degree of accuracy [51]. Collectively, these findings strongly suggest that the irreversible deformations observed in the early phases of MV remodeling can be attributed mainly to *sustained* mechanical distentions and subsequent scission-healing mechanisms in the extracellular matrix surrounding the collagen fibers.

4.3. Potential biological mechanisms

A range of biological mechanisms have also been demonstrated to direct growth and remodelling of the MV following long-term shifts in homeostasis. It has been established that the primary agents of growth and remodelling are the MV interstitial cells (MVICs), which in their quiescent state typically regulate extracellular matrix (ECM) production and degradation, principally by synthesizing and secreting interstitial collagen. However, under certain conditions, MVICs can become activated and adopt myofibroblast-like characteristics that aid in valvular remodelling. Though this activation under nonpathological shifts in boundary conditions (such as pregnancy) can support necessary adaptation to preserve the critical function of the MV [69], pathological dysregulation of this process (typically due to mechanical overload) can lead to fibrosis, stiffening and thickening of the valve tissue [65, 70–73]. Moreover, MV endothelial cells (MVECs), which line the outer layer of the leaflet tissue, can also be induced to migrate into the ECM and change phenotype into MVICs, which can later transform into myofibroblasts. This process is known as endothelial-to-mesenchymal transition (EndMT), which at certain levels can be a normal pathway to replenish MVICs and ensure appropriate valve function. When the endothelial layer's integrity is compromised by stimuli such as mechanical stress or inflammation (e.g., after a myocardial infarction), circulating leukocytes and myeloid cells can infiltrate the valve tissue and differentiate into macrophages. These macrophages release inflammatory cytokines including TGF-β, promoting valve inflammation and triggering abnormal EndMT and subsequent tissue remodelling [74].

Interestingly, in myxomatous MV tissue as can be found in primary MR, the mechanism of remodelling is slightly different, likely due to the difference in mechanical loading. Typically, myxomatous MVs, which usually present with MV prolapse, are under abnormally low mechanical loading, especially compared to tethered SMR MVs. In contrast to fibrotic remodeling, myxomatous MVs have been shown to be more extensible, with lower stiffness [75]. Mainly, myxomatous-type remodeling seems to present with significantly elevated concentrations of glycosaminoglycans (GAGs) and water content, contributing to the weaker overall mechanical profile of these tissues [76, 77]. Overall, these studies thoroughly demonstrate that in *both* primary and secondary MR, the MV tissue is far from normal and constitutes an already deteriorated initial state which repair techniques further perturb.

The MV has been shown to exhibit adverse remodeling processes in various clinically relevant pathologies, including secondary MR [66, 77–80], MI [22, 74, 81], dilated cardiomyopathy

[82–84], and heart failure [24, 28]. In all these conditions, where the MV is subject to altered loading patterns due to annular dilatation, papillary muscle displacement, hemodynamic stressors, or some combination of the above, common findings included increased leaflet area and thickness, elevated collagen mass fraction and TGF-β expression, and progressive tissue stiffening, all indicating a fibrotic-type remodeling cascade. Clinically, Nishino et al. showed in a longitudinal echocardiographic study of patients' MVs post-MI and the onset of ischemic MR that patients with persistent ischemic MR presented with larger annuli, increased tenting and a reduced leaflet area/annular ratio compared to patients without significant IMR. Additionally, the MV leaflets were thicker in patients with chronic IMR compared to acute IMR, with increased fibrosis [29].

4.4. Remodeling mechanisms in the context of TEER

Within this context, TEER has enormous potential to trigger adverse leaflet remodelling. First, we and others have previously shown that TEER locally increases the deformation experienced in the leaflet tissue, a finding that was echoed in this work (Section 3.2) [48]. As this new functional state is permanent, there is a sustained shift in stress conditions of the MV leaflets which can certainly lead to mechanically driven permanent set-type mechanisms in the months following repair. Second, the design of the MitraClip grippers includes small barbs designed to hook into the leaflet tissue to prevent device detachment. Certainly these, along with the cyclical friction of the arms against the tissue during the cardiac cycle, can compromise the integrity of the endothelial layer and initiate an immune-mediated inflammatory response that triggers EndMT and fibrosis *in the long-term*. Indeed, explanted MitraClip devices from patients undergoing reintervention with mitral replacement show on gross examination the substantial formation of fibrotic scar tissue around the device, as well as immune cell infiltration upon histological analysis over 8-12 months post-implant [85, 86]. Ladich et al. explanted devices over 1 to 1878 days from implant and observed four phases of physiological healing: platelet and fibrin deposition, inflammation, granulation tissue, and finally, fibrous encapsulation [87]. Notably, around the 90-day timepoint corresponding to the follow-up timepoint in this study, the authors found evidence of granulation tissue and early fibrous encapsulation. However, these findings are limited to the tissue immediately surrounding the device, and no histological analyses have been done to our knowledge on explanted, post-TEER MV leaflet tissue in general.

Finally, it is important to note that TEER is typically performed on patients with very advanced MR who are too ill to tolerate surgical intervention. For this study, which focuses mainly on the subacute/early chronic phases post-TEER, it is in this context that biological mechanisms play a key role. In contrast to other studies and to our earlier work invovling ovine MVs, the pre-operative biomechanical state of these patients' MVs is *far from normal*. Either the collagen is intrinscially damaged by myxomatous or rheumatic processes, or continued dilatation of the annulus and/or ventricle have placed the MV in an abnormal stress state, or both. Over the

chronic period post-MR, both mechanically-driven plasticity and biological mechanisms like inflammation and MVIC activation have been involved in altering the pre-operative state of the MV. Therefore, the imposition of the TEER device, with its own related mechanical and inflammatory triggers, onto tissue which already has already undergone MR-induced plasticity and features activated MVICs and dysregulated EndMT and fibrotic pathways, creates an environment primed for continued adverse remodelling [74].

4.5. Clinical implications

This study, which confirms the presence of MV plasticity in patients who have undergone TEER, has major clinical implications. First, we have laid the groundwork to establish a link between the TEER intervention and the onset of plastic deformation in patient MV tissue. This relationship is already innately understood in the clinic; the general avoidance of the long, narrow XT MitraClip [64] and the very existence of the PASCAL device, which in almost every design element (flexible nitinol material, paddle-shaped arms, central spacer) seeks to minimize the stress imposed on the leaflets, affirm the prevailing clinical concern regarding the post-operative functional state of the valve. With our computational techniques, we are able to interrogate the in vivo kinematics of the patient MV, and importantly, directly *quantify* the intuitive insights that are already guiding the progression of TEER as an intervention.

As such, these simulations are a valuable tool towards precisely optimizing the TEER procedural to achieve optimal durability and efficacy in the patient population. Importantly, by enabling the analysis of tissue plasticity, the approaches introduced in this work augment the assessment of TEER success by also offering a long-term view of post-repair MV function. Mitral valve plasticity, particularly with this disease and intervention, is highly complex, and consequently, distinguishing an exact causative mechanism linking patient or operative characteristics to the magnitude of plasticity is a significant task. For example, we and others have shown that even in FMR, which is traditionally thought of as an externally driven etiology with "normal" leaflet tissue, the MV undergoes pathological functional shifts, such as marked radial stiffening [19, 24, 28]. As such, the degree of MR progression would also be important to consider when contextualizing plasticity post-TEER. Moreover, from an intervention point of view, not only does the clip choice matter, but also their placement in the MV (especially if other pathologies, such as calcification, are already present). Though this may seem like a herculean task to optimize so many interconnected variables, computational simulations are well-suited to address this challenges, and our simulation techniques as presented in this work represent a crucial preliminary step towards this objective.

Finally, this initial study has shown not only our capacity to observe plasticity, but also lays the groundwork for *time-evolving predictions* of MV leaflet tissue behavior. Our correlation results as presented in Section 3.5 demonstrate that for each patient, the follow-up systolic state is directed by the initial pre-operative state and immediate post-operative function. Moreover,

plasticity itself, as can be expected, is influenced by post-operative systolic function, which inherently includes the specifics of the clip configuration, when referenced to the post-operative end-diastolic state (the same reference as plasticity). We have already demonstrated our ability to predict the post-operative state after undersized ring annuloplasty [67], and to simulate the progression of plasticity over time after myocardial infarction [51]. By building on the protocols presented in these two works, as well as the insights derived from this study, we are currently developing a modeling and simulation pipeline that can predict MV function over time using standard-of-care pre-operative imaging alone.

4.6. Limitations

While comprehensive, this study has certain limitations. Mainly, the sample size of the patient cohort is small, though greater the required sample size ($n = 4$) to distinguish the presence of plasticity with 95% power. However, we are not able to make any correlations between the level of plasticity and patient outcomes. Moreover, the heterogeneity of the patient cohort with respect to clip type and placement also complicates any attempt to relate plasticity magnitude with clip configuration. The principal hurdle in terms of sample size is quite simply the reluctance of patients to undergo an additional, medically unnecessary invasive procedure (the 3-month TEE imaging). Nevertheless, even in its modest size, this patient cohort represents the first such longitudinal imaging dataset acquired solely for computational analysis, rather than clinical trial followup, and has still facilitated important revelations regarding the MV tissue and functional response to TEER. Furthermore, this is strictly an in vivo, imaging-based study, so we have not conducted in vitro tissue analysis on explanted tissue samples. Therefore, though we are able to hypothesize certain tissue-level mechanisms potentially driving MV plasticity, additional mechanical and histological studies on explanted patient MV tissue would be needed to confirm and expand the present findings. However, it is important to note that an image-based analysis presents a significant advantage in that this approach allows us to investigate the *in vivo behavior of diseased human MVs*, inherently accounting for all the complex mechanisms underscoring MV physiology, such as leaflet prestrain, that we have found to be so critical to the accurate analysis of its function [88, 89].

4.7. Conclusions and future directions

In summary, this study quantified for the first time in vivo MV leaflet plasticity following transcatheter edge-to-edge repair in humans. Our findings not only confirm the presence of plastic deformation, but also offer strong evidence that this plasticity is primarily driven by the TEER procedure itself, rather than other organ-level shifts in loading or boundary conditions. This study emphasizes once again the importance of an individualized approach to MV treatment optimization, but with a holistic focus on all aspects of MV function, with the objective to ensure the best possible *long-term* outcomes for each patient.

The outcomes of this study further emphasize the need for and value of image-based computational methods. Such techniques allow for the in vivo assessment of native MV function in human patients on an individual basis, insights that would not be possible with purely in vitro experimentation or clinical imaging alone. Moreover, the use of clinical imaging as the basis of the modeling allows for the future integration of this analysis pipeline directly into the clinical workflow, further amplifying the utility of computational methods in real-world patient scenarios. Specifically, this work also further demonstrates the capacity of our computational methods to finely interrogate multiple key aspects of the in vivo function of the human MV and lays the groundwork for future predictive, time-evolving simulations of post-repair MV function. Importantly, these results imply that, with an appropriate predictive model of the post-TEER functional state, longer term responses to MV TEER can be predicted.

5. Conflicts of Interest

None.

6. Acknowledgments

TBD

References

References

[1] W. Coleman, E. Weidman-Evans, R. Clawson, Diagnosing and managing mitral regurgitation, JAAPA 30 (6) (2017) 11–14.

[2] R. A. Nishimura, A. Vahanian, M. F. Eleid, M. J. Mack, Mitral valve disease—current management and future challenges, The Lancet 387 (10025) (2016) 1324–1334.

[3] J. Hausleiter, T. J. Stocker, M. Adamo, N. Karam, M. J. Swaans, F. Praz, Mitral valve transcatheter edge-to-edge repair, EuroIntervention 18 (12) (2023) 957.

[4] D. Messika-Zeitoun, P. Candolfi, A. Vahanian, V. Chan, I. G. Burwash, J.-F. Philippon, J.-M. Toussaint, P. Verta, T. E. Feldman, B. Iung, et al., Dismal outcomes and high societal burden of mitral valve regurgitation in france in the recent era: A nationwide perspective, Journal of the American Heart Association 9 (15) (2020) e016086.

[5] R. Prakash, M. Horsfall, A. Markwick, M. Pumar, L. Lee, A. Sinhal, M. X. Joseph, D. P. Chew, Prognostic impact of moderate or severe mitral regurgitation (mr) irrespective of concomitant comorbidities: a retrospective matched cohort study, BMJ open 4 (7) (2014) e004984.

[6] T. Feldman, H. S. Wasserman, H. C. Herrmann, W. Gray, P. C. Block, P. Whitlow, F. St. Goar, L. Rodriguez, F. Silvestry, A. Schwartz, et al., Percutaneous mitral valve repair using the edge-to-edge technique: six-month results of the everest phase i clinical trial, Journal of the American College of Cardiology 46 (11) (2005) 2134–2140.

[7] O. Alfieri, F. Maisano, M. De Bonis, P. L. Stefano, L. Torracca, M. Oppizzi, G. La Canna, The double-orifice technique in mitral valve repair: a simple solution for complex problems, The Journal of thoracic and cardiovascular surgery 122 (4) (2001) 674–681.

[8] T. Feldman, E. Foster, D. D. Glower, S. Kar, M. J. Rinaldi, P. S. Fail, R. W. Smalling, R. Siegel, G. A. Rose, E. Engeron, et al., Percutaneous repair or surgery for mitral regurgitation, New England Journal of Medicine 364 (15) (2011) 1395–1406.

[9] T. Feldman, S. Kar, S. Elmariah, S. C. Smart, A. Trento, R. J. Siegel, P. Apruzzese, P. Fail, M. J. Rinaldi, R. W. Smalling, et al., Randomized comparison of percutaneous repair and surgery for mitral regurgitation: 5-year results of everest ii, Journal of the American College of Cardiology 66 (25) (2015) 2844–2854.

[10] J.-F. Obadia, D. Messika-Zeitoun, G. Leurent, B. Iung, G. Bonnet, N. Piriou, T. Lefèvre, C. Piot, F. Rouleau, D. Carrié, et al., Percutaneous repair or medical treatment for secondary mitral regurgitation, New England Journal of Medicine 379 (24) (2018) 2297–2306.

[11] G. W. Stone, J. Lindenfeld, W. T. Abraham, S. Kar, D. S. Lim, J. M. Mishell, B. Whisenant, P. A. Grayburn, M. Rinaldi, S. R. Kapadia, et al., Transcatheter mitral-valve repair in patients with heart failure, New England Journal of Medicine 379 (24) (2018) 2307–2318.

[12] C. M. Otto, R. A. Nishimura, R. O. Bonow, B. A. Carabello, J. P. Erwin III, F. Gentile, H. Jneid, E. V. Krieger, M. Mack, C. McLeod, et al., 2020 acc/aha guideline for the management of patients with valvular heart disease: executive summary: a report of the american college of cardiology/american heart association joint committee on clinical practice guidelines, Journal of the American College of Cardiology 77 (4) (2021) 450–500.

[13] A. Vahanian, F. Beyersdorf, F. Praz, M. Milojevic, S. Baldus, J. Bauersachs, D. Capodanno, L. Conradi, M. De Bonis, R. De Paulis, et al., 2021 esc/eacts guidelines for the management of valvular heart disease: developed by the task force for the management of valvular heart disease of the european society of cardiology (esc) and the european association for cardio-thoracic surgery (eacts), European heart journal 43 (7) (2022) 561–632.

[14] T. Salvatore, F. Ricci, G. D. Dangas, B. S. Rana, L. Ceriello, L. Testa, M. Y. Khanji, A. L. Caterino, C. Fiore, A. Popolo Rubbio, et al., Selection of the optimal candidate to mitraclip for secondary mitral regurgitation: beyond mitral valve morphology, Frontiers in Cardiovascular Medicine 8 (2021) 585415.

[15] R. S. von Bardeleben, P. Mahoney, M. A. Morse, M. J. Price, P. Denti, F. Maisano, J. H. Rogers, M. Rinaldi, F. De Marco, W. Rollefson, et al., 1-year outcomes with fourth-generation mitral valve transcatheter edge-to-edge repair from the expand g4 study, Cardiovascular Interventions 16 (21) (2023) 2600–2610.

[16] R. L. Smith, D. S. Lim, L. D. Gillam, F. Zahr, S. Chadderdon, A. N. Rassi, R. Makkar, S. Goldman, V. Rudolph, J. Hermiller, et al., 1-year outcomes of transcatheter edge-to-edge repair in anatomically complex degenerative mitral regurgitation patients, Cardiovascular Interventions 16 (23) (2023) 2820–2832.

[17] S. H. McKellar, J. Harkness, B. B. Reid, N. K. Sekaran, H. T. May, B. K. Whisenant, Residual or recurrent mitral regurgitation predicts mortality following transcatheter edge-to-edge mitral valve repair, JTCVS open 16 (2023) 191–206.

[18] M. De Bonis, E. Lapenna, N. Buzzatti, G. La Canna, P. Denti, F. Pappalardo, D. Schiavi, A. Pozzoli, M. Cioni, G. Di Giannuario, et al., Optimal results immediately after mitraclip therapy or surgical edge-to-edge repair for functional mitral regurgitation: are they really stable at 4 years?, European Journal of Cardio-Thoracic Surgery 50 (3) (2016) 488–494.

[19] D. P. Howsmon, B. V. Rego, E. Castillero, S. Ayoub, A. H. Khalighi, R. C. Gorman, J. H. Gorman III, G. Ferrari, M. S. Sacks, Mitral valve leaflet response to ischaemic mitral regur-

gitation: from gene expression to tissue remodelling, Journal of the Royal Society Interface 17 (166) (2020) 20200098.

[20] S. Ayoub, C.-H. Lee, K. H. Driesbaugh, W. Anselmo, C. T. Hughes, G. Ferrari, R. C. Gorman, J. H. Gorman, M. S. Sacks, Regulation of valve interstitial cell homeostasis by mechanical deformation: implications for heart valve disease and surgical repair, Journal of The Royal Society Interface 14 (135) (2017) 20170580.

[21] B. V. Rego, A. H. Khalighi, E. K. Lai, R. C. Gorman, J. H. Gorman, M. S. Sacks, In vivo assessment of mitral valve leaflet remodelling following myocardial infarction, Scientific reports 12 (1) (2022) 1–16.

[22] J. P. Dal-Bianco, E. Aikawa, J. Bischoff, J. L. Guerrero, J. Hjortnaes, J. Beaudoin, C. Szymanski, P. E. Bartko, M. M. Seybolt, M. D. Handschumacher, et al., Myocardial infarction alters adaptation of the tethered mitral valve, Journal of the American College of Cardiology 67 (3) (2016) 275–287.

[23] R. A. Levine, A. A. Hagége, D. P. Judge, M. Padala, J. P. Dal-Bianco, E. Aikawa, J. Beaudoin, J. Bischoff, N. Bouatia-Naji, P. Bruneval, et al., Mitral valve disease—morphology and mechanisms, Nature reviews cardiology 12 (12) (2015) 689–710.

[24] K. J. Grande-Allen, J. E. Barber, K. M. Klatka, P. L. Houghtaling, I. Vesely, C. S. Moravec, P. M. McCarthy, Mitral valve stiffening in end-stage heart failure: evidence of an organic contribution to functional mitral regurgitation, The Journal of thoracic and cardiovascular surgery 130 (3) (2005) 783–790.

[25] M. Chaput, M. D. Handschumacher, F. Tournoux, L. Hua, J. L. Guerrero, G. J. Vlahakes, R. A. Levine, Mitral leaflet adaptation to ventricular remodeling: occurrence and adequacy in patients with functional mitral regurgitation, Circulation 118 (8) (2008) 845–52. doi:10.1161/circulationaha.107.749440.
URL http://circ.ahajournals.org/content/118/8/845.full.pdf

[26] P. Debonnaire, I. Al Amri, D. P. Leong, E. Joyce, S. Katsanos, V. Kamperidis, M. J. Schalij, J. J. Bax, N. A. Marsan, V. Delgado, Leaflet remodelling in functional mitral valve regurgitation: characteristics, determinants, and relation to regurgitation severity, European Heart Journal-Cardiovascular Imaging 16 (3) (2015) 290–299.

[27] K. Saito, H. Okura, N. Watanabe, K. Obase, T. Tamada, T. Koyama, A. Hayashida, Y. Neishi, T. Kawamoto, K. Yoshida, Influence of chronic tethering of the mitral valve on mitral leaflet size and coaptation in functional mitral regurgitation, JACC: Cardiovascular Imaging 5 (4) (2012) 337–345.

[28] K. J. Grande-Allen, A. G. Borowski, R. W. Troughton, P. L. Houghtaling, N. R. DiPaola, C. S. Moravec, I. Vesely, B. P. Griffin, Apparently normal mitral valves in patients with heart failure demonstrate biochemical and structural derangements: an extracellular matrix and echocardiographic study, Journal of the American College of Cardiology 45 (1) (2005) 54–61.

[29] S. Nishino, N. Watanabe, T. Gi, N. Kuriyama, Y. Shibata, Y. Asada, Longitudinal evaluation of mitral valve leaflet remodeling after acute myocardial infarction: serial quantitation of valve geometry using real-time 3-dimensional echocardiography, Circulation: Cardiovascular Imaging 13 (12) (2020) e011396.

[30] J. P. Dal-Bianco, R. A. Levine, J. Hung, Mitral regurgitation postinfarction: the mitral valve adapts to the times (2020).

[31] T. Mansi, I. Voigt, B. Georgescu, X. Zheng, E. A. Mengue, M. Hackl, R. I. Ionasec, T. Noack, J. Seeburger, D. Comaniciu, An integrated framework for finite-element modeling of mitral valve biomechanics from medical images: application to mitralclip intervention planning, Medical image analysis 16 (7) (2012) 1330–1346.

[32] R. Kamakoti, Y. Dabiri, D. D. Wang, J. Guccione, G. S. Kassab, Numerical simulations of mitraclip placement: clinical implications, Scientific reports 9 (1) (2019) 15823.

[33] Y. Dabiri, V. S. Mahadevan, J. M. Guccione, G. S. Kassab, A simulation study of the effects of number and location of mitraclips on mitral regurgitation, JACC: Advances 1 (1) (2022) 100015.

[34] Y. Dabiri, J. Yao, V. S. Mahadevan, D. Gruber, R. Arnaout, W. Gentzsch, J. M. Guccione, G. S. Kassab, Mitral valve atlas for artificial intelligence predictions of mitraclip intervention outcomes, Frontiers in Cardiovascular Medicine 8 (2021) 759675.

[35] F. Sturla, A. Redaelli, G. Puppini, F. Onorati, G. Faggian, E. Votta, Functional and biomechanical effects of the edge-to-edge repair in the setting of mitral regurgitation: consolidated knowledge and novel tools to gain insight into its percutaneous implementation, Cardiovascular Engineering and Technology 6 (2015) 117–140.

[36] F. Sturla, R. Vismara, M. Jaworek, E. Votta, P. Romitelli, O. A. Pappalardo, F. Lucherini, C. Antona, G. B. Fiore, A. Redaelli, In vitro and in silico approaches to quantify the effects of the mitraclip® system on mitral valve function, Journal of biomechanics 50 (2017) 83–92.

[37] A. E. Morgan, J. L. Pantoja, J. Weinsaft, E. Grossi, J. M. Guccione, L. Ge, M. Ratcliffe, Finite element modeling of mitral valve repair, Journal of biomechanical engineering 138 (2) (2016) 021009.

[38] B. Prescott, C. J. Abunassar, K. P. Baxevanakis, L. Zhao, Computational evaluation of mitral valve repair with mitraclip, Vessel Plus 3 (13) (2019) 1–10.

[39] K. Vellguth, F. Barbieri, M. Reinthaler, M. Kasner, U. Landmesser, T. Kuehne, A. Hennemuth, L. Walczak, L. Goubergrits, Effect of transcatheter edge-to-edge repair device position on diastolic hemodynamic parameters: An echocardiography-based simulation study, Frontiers in Cardiovascular Medicine 9 (2022) 915074.

[40] Y. Dabiri, V. S. Mahadevan, J. M. Guccione, G. S. Kassab, Machine learning used for simulation of mitraclip intervention: A proof-of-concept study, Frontiers in Genetics 14 (2023) 1142446.

[41] S. Pasta, In silico analysis of the mitraclip in a realistic human left heart model, Prosthesis 5 (3) (2023) 876–887.

[42] F. Kong, A. Caballero, R. McKay, W. Sun, Finite element analysis of mitraclip procedure on a patient-specific model with functional mitral regurgitation, Journal of biomechanics 104 (2020) 109730.

[43] A. Caballero, W. Mao, R. McKay, R. T. Hahn, W. Sun, A comprehensive engineering analysis of left heart dynamics after mitraclip in a functional mitral regurgitation patient, Frontiers in physiology 11 (2020) 432.

[44] A. Caballero, T. Qin, R. T. Hahn, R. McKay, W. Sun, Quantification of mitral regurgitation after transcatheter edge-to-edge repair: Comparison of echocardiography and patient-specific in silico models, Computers in Biology and Medicine 148 (2022) 105855.

[45] A. Miyata, T. Miyamoto, M. Imai, Y. Sato, Preprocedural simulation of a mitral transcatheter edge-to-edge repair using computed tomography imaging, European Heart Journal 44 (Supplement_2) (2023) ehad655–2262.

[46] R. Errthum, A. Caballero, R. McKay, W. Sun, Comparative computational analysis of pascal and mitraclip implantation in a patient-specific functional mitral regurgitation model, Computers in Biology and Medicine 136 (2021) 104767.

[47] J. Ooida, N. Kiyohara, H. Noguchi, Y. Oguchi, K. Nagane, T. Sakaguchi, G. Aoyama, F. Shige, J. V. Chapman, M. Asami, et al., An in silico model for predicting the efficacy of edge-to-edge repair for mitral regurgitation, Journal of biomechanical engineering 146 (2) (2024).

[48] N. T. Simonian, H. Liu, S. Vakamudi, M. J. Pirwitz, A. M. Pouch, J. H. Gorman III, R. C. Gorman, M. S. Sacks, Patient-specific quantitative in-vivo assessment of human mitral valve

leaflet strain before and after mitraclip repair, Cardiovascular Engineering and Technology 14 (5) (2023) 677–693.

[49] G. Gaidulis, M. Padala, A 3d echo derived computational modeling platform to predict patient-specific outcomes after transcatheter edge-to-edge repair, Journal of the American College of Cardiology 81 (8_Supplement) (2023) 1956–1956.

[50] B. V. Rego, A. H. Khalighi, A. Drach, E. K. Lai, A. M. Pouch, R. C. Gorman, J. H. Gorman III, M. S. Sacks, A noninvasive method for the determination of in vivo mitral valve leaflet strains, International journal for numerical methods in biomedical engineering 34 (12) (2018) e3142.

[51] B. V. Rego, A. H. Khalighi, J. H. Gorman, R. C. Gorman, M. S. Sacks, Simulation of mitral valve plasticity in response to myocardial infarction, Annals of Biomedical Engineering (2022) 1–17.

[52] S. Ludwig, D. Kalbacher, W. B. Ali, J. Weimann, M. Adam, A. Duncan, J. G. Webb, S. Windecker, M. Orban, C. Giannini, et al., Transcatheter mitral valve replacement or repair for secondary mitral regurgitation: a propensity score-matched analysis, European journal of heart failure 25 (3) (2023) 399–410.

[53] D. W. Muller, P. Sorajja, A. Duncan, B. Bethea, G. Dahle, P. Grayburn, V. Babaliaros, M. Guerrero, V. H. Thourani, F. Bedogni, et al., 2-year outcomes of transcatheter mitral valve replacement in patients with severe symptomatic mitral regurgitation, Journal of the American College of Cardiology 78 (19) (2021) 1847–1859.

[54] W. Ningyan, Y. K. Keong, Percutaneous edge-to-edge mitral valve repair for functional mitral regurgitation, International Journal of Heart Failure 4 (2) (2022) 55.

[55] N. T. Simonian, H. Liu, A. M. Pouch, J. H. Gorman III, R. C. Gorman, M. S. Sacks, Quantitative in vivo assessment of human mitral valve coaptation area after undersized ring annuloplasty repair for ischemic mitral regurgitation, JTCVS Techniques (2022).

[56] H. Narang, B. V. Rego, A. H. Khalighi, A. Aly, A. M. Pouch, R. C. Gorman, J. H. Gorman III, M. S. Sacks, Pre-surgical prediction of ischemic mitral regurgitation recurrence using in vivo mitral valve leaflet strains, Annals of Biomedical Engineering 49 (12) (2021) 3711–3723.

[57] W. Zhang, S. Ayoub, J. Liao, M. S. Sacks, A meso-scale layer-specific structural constitutive model of the mitral heart valve leaflets, Acta Biomater 32 (2016) 238–55. doi:10.1016/j.actbio.2015.12.001.
URL http://www.ncbi.nlm.nih.gov/pubmed/26712602

[58] C. E. Eckert, B. Zubiate, M. Vergnat, J. H. Gorman, 3rd, R. C. Gorman, M. S. Sacks, In vivo dynamic deformation of the mitral valve annulus, Ann Biomed Eng 37 (9) (2009) 1757–71. doi:10.1007/s10439-009-9749-3.
URL http://www.ncbi.nlm.nih.gov/entrez/query.fcgi?cmd=Retrieve&db=PubMed&dopt=Citation&list_uids=19585241

[59] K. Hashiguchi, Nonlinear continuum mechanics for finite elasticity-plasticity: Multiplicative decomposition with subloading surface model, Elsevier, 2020.

[60] V. A. Lubarda, Elastoplasticity theory, CRC press, 2001.

[61] R. M. Lang, L. P. Badano, V. Mor-Avi, J. Afilalo, A. Armstrong, L. Ernande, F. A. Flachskampf, E. Foster, S. A. Goldstein, T. Kuznetsova, et al., Recommendations for cardiac chamber quantification by echocardiography in adults: an update from the american society of echocardiography and the european association of cardiovascular imaging, European Heart Journal-Cardiovascular Imaging 16 (3) (2015) 233–271.

[62] I. Al Amri, P. Debonnaire, F. van der Kley, M. J. Schalij, J. J. Bax, N. A. Marsan, V. Delgado, Acute effect of mitraclip implantation on mitral valve geometry in patients with functional mitral regurgitation: insights from three-dimensional transoesophageal echocardiography, EuroIntervention 11 (13) (2016) 1554–1561.

[63] F. Hidalgo, D. Mesa, M. Ruiz, M. Delgado, S. Rodríguez, L. Pardo, M. Pan, A. Lopez, M. A. Romero, J. S. de Lezo, Effects of mitral annulus remodeling following mitraclip procedure on reduction of functional mitral regurgitation, Revista Española de Cardiología (English Edition) 69 (11) (2016) 1020–1025.

[64] F. Praz, M. G. Winkel, N. P. Fam, A new age for transcatheter mitral valve repair: the complexity of choice (2020).

[65] M. K. Rausch, F. A. Tibayan, D. C. Miller, E. Kuhl, Evidence of adaptive mitral leaflet growth, J Mech Behav Biomed Mater 15 (2012) 208–17. doi:10.1016/j.jmbbm.2012.07.001.
URL http://www.ncbi.nlm.nih.gov/pubmed/23159489

[66] M. Chaput, M. D. Handschumacher, J. L. Guerrero, G. Holmvang, J. P. Dal-Bianco, S. Sullivan, G. J. Vlahakes, J. Hung, R. A. Levine, Mitral leaflet adaptation to ventricular remodeling: prospective changes in a model of ischemic mitral regurgitation, Circulation 120 (11 Suppl) (2009) S99–103. doi:10.1161/CIRCULATIONAHA.109.844019.
URL http://www.ncbi.nlm.nih.gov/pubmed/19752393

[67] H. Liu, N. T. Simonian, A. M. Pouch, P. A. Iaizzo, I. Gorman, Joseph H., R. C. Gorman, M. S. Sacks, A Computational Pipeline for Patient-Specific Prediction of the Postoperative Mitral Valve Functional State, Journal of Biomechanical Engineering 145 (11) (2023) 111002. arXiv:https://asmedigitalcollection.asme.org/biomechanical/article-pdf/145/11/111002/7032781/bio_145_11_111002.pdf, doi:10.1115/1.4062849.
URL https://doi.org/10.1115/1.4062849

[68] W. Zhang, M. S. Sacks, Modeling the response of exogenously crosslinked tissue to cyclic loading: The effects of permanent set 75 336–350.

[69] B. V. Rego, S. M. Wells, C.-H. Lee, M. S. Sacks, Mitral valve leaflet remodelling during pregnancy: insights into cell-mediated recovery of tissue homeostasis, Journal of The Royal Society Interface 13 (125) (2016) 20160709.

[70] A. Sielicka, E. L. Sarin, W. Shi, F. Sulejmani, D. Corporan, K. Kalra, V. H. Thourani, W. Sun, R. A. Guyton, M. Padala, Pathological remodeling of mitral valve leaflets from unphysiologic leaflet mechanics after undersized mitral annuloplasty to repair ischemic mitral regurgitation, Journal of the American Heart Association 7 (21) (2018) e009777.

[71] J. P. Dal-Bianco, E. Aikawa, J. Bischoff, J. L. Guerrero, M. D. Handschumacher, S. Sullivan, B. Johnson, J. S. Titus, Y. Iwamoto, J. Wylie-Sears, et al., Active adaptation of the tethered mitral valve: insights into a compensatory mechanism for functional mitral regurgitation, Circulation 120 (4) (2009) 334–342.

[72] B. P. Kruithof, L. Paardekooper, Y. L. Hiemstra, M.-J. Goumans, M. Palmen, V. Delgado, R. J. Klautz, N. Ajmone Marsan, Stress-induced remodelling of the mitral valve: a model for leaflet thickening and superimposed tissue formation in mitral valve disease, Cardiovascular research 116 (5) (2020) 931–943.

[73] R. K. Balachandran, V. H. Barocas, Contribution of saccadic motion to intravitreal drug transport: theoretical analysis, Pharm Res 28 (5) (2011) 1049–64. doi:10.1007/s11095-010-0356-7.
URL http://www.ncbi.nlm.nih.gov/pubmed/21258958

[74] A. M. Calafiore, A. Totaro, N. Testa, C. Sacra, G. Castellano, S. Guarracini, M. Di Marco, S. Prapas, M. Gaudino, R. Lorusso, et al., The secret life of the mitral valve, Journal of Cardiac Surgery 36 (1) (2021) 247–259.

[75] K. Grande-Allen, Fibrotic vs. myxomatous remodeling of mitral valves, in: The 26th Annual International Conference of the IEEE Engineering in Medicine and Biology Society, Vol. 2, IEEE, 2004, pp. 3737–3740.

[76] K. J. Grande-Allen, B. P. Griffin, N. B. Ratliff, D. M. Cosgrove, I. Vesely, Glycosaminoglycan profiles of myxomatous mitral leaflets and chordae parallel the severity of mechanical alterations, Journal of the American College of Cardiology 42 (2) (2003) 271–277.

[77] P. S. Connell, A. F. Azimuddin, S. E. Kim, F. Ramirez, M. S. Jackson, S. H. Little, K. J. Grande-Allen, Regurgitation hemodynamics alone cause mitral valve remodeling characteristic of clinical disease states in vitro, Annals of biomedical engineering 44 (2016) 954–967.

[78] K. C. El-Tallawi, P. Zhang, R. Azencott, J. He, J. Xu, E. L. Herrera, J. Jacob, M. Chamsi-Pasha, G. M. Lawrie, W. A. Zoghbi, Mitral valve remodeling and strain in secondary mitral regurgitation: comparison with primary regurgitation and normal valves, Cardiovascular Imaging 14 (4) (2021) 782–793.

[79] E. H. Stephens, T. C. Nguyen, A. Itoh, N. B. Ingels Jr, D. C. Miller, K. J. Grande-Allen, The effects of mitral regurgitation alone are sufficient for leaflet remodeling, Circulation 118 (14_suppl_1) (2008) S243–S249.

[80] F. Mahmood, Z. O. Knio, L. Yeh, R. Amir, R. Matyal, A. Mashari, R. C. Gorman, J. H. Gorman III, K. R. Khabbaz, Regional heterogeneity in the mitral valve apparatus in patients with ischemic mitral regurgitation, The Annals of thoracic surgery 103 (4) (2017) 1171–1177.

[81] J. Beaudoin, J. P. Dal-Bianco, E. Aikawa, J. Bischoff, J. L. Guerrero, S. Sullivan, P. E. Bartko, M. D. Handschumacher, D.-H. Kim, J. Wylie-Sears, et al., Mitral leaflet changes following myocardial infarction: clinical evidence for maladaptive valvular remodeling, Circulation: Cardiovascular Imaging 10 (11) (2017) e006512.

[82] S. Yoshida, S. Fukushima, S. Miyagawa, Y. Yoshikawa, H. Hata, S. Saito, T. Saito, K. Domae, N. Kashiyama, R. Matsuura, et al., The adaptive remodeling of the anterior mitral leaflet and chordae tendineae is associated with mitral valve function in advanced ischemic and nonischemic dilated cardiomyopathy, International Heart Journal 59 (5) (2018) 959–967.

[83] T. A. Timek, D. T. Lai, P. Dagum, D. Liang, G. T. Daughters, N. B. Ingels Jr, D. C. Miller, Mitral leaflet remodeling in dilated cardiomyopathy, Circulation 114 (1_supplement) (2006) I–518.

[84] E. H. Stephens, T. A. Timek, G. T. Daughters, J. J. Kuo, A. M. Patton, L. S. Baggett, N. B. Ingels, D. C. Miller, K. J. Grande-Allen, Significant changes in mitral valve leaflet matrix composition and turnover with tachycardia-induced cardiomyopathy, Circulation 120 (11_suppl_1) (2009) S112–S119.

[85] P. Mazur, A. Arghami, C. Zheng, M. Alkhouli, H. V. Schaff, J. Dearani, R. C. Daly, K. Greason, J. A. Crestanello, Mitral valve surgery after failed transcatheter edge-to-edge repair, JTCVS techniques 14 (2022) 79–88.

[86] M. O. Schmiady, M. Taramasso, F. Maisano, M. Sigler, Mitral valve surgery after mitraclip® implantation: what histopathology can tell us?, European Heart Journal 41 (38) (2020) 3767–3767.

[87] E. Ladich, M. B. Michaels, R. M. Jones, E. McDermott, L. Coleman, J. Komtebedde, D. Glower, M. Argenziano, T. Feldman, M. Nakano, et al., Pathological healing response of explanted mitraclip devices, Circulation 123 (13) (2011) 1418–1427.

[88] R. Amini, C. E. Eckert, K. Koomalsingh, J. McGarvey, M. Minakawa, J. H. Gorman, R. C. Gorman, M. S. Sacks, On the in vivo deformation of the mitral valve anterior leaflet: effects of annular geometry and referential configuration, Ann Biomed Eng 40 (7) (2012) 1455–67. doi:10.1007/s10439-012-0524-5.
URL http://www.ncbi.nlm.nih.gov/pubmed/22327292

[89] H. Liu, M. S. Sacks, N. T. Simonian, J. H. Gorman III, R. C. Gorman, Simulated effects of acute left ventricular myocardial infarction on mitral regurgitation in an ovine model, Journal of Biomechanical Engineering 146 (10) (2024) 101009.